Kansas Geological Survey

Approximate Analysis of Groundwater Mineralization Due to Discontinuity in an Impermeable Layer

Part 2: Seepage of Saltwater through a Semiconfining Discontinuity

By

Hillel Rubin* and Robert W. Buddemeier
Kansas Geological Survey, The University of Kansas
Lawrence, KS 66047

Kansas Geological Survey Open File Report 98-32

July 26, 1998

GEOHYDROLOGY

The University of Kansas, Lawrence, KS 66047 Tel. (785) 864-3965

Kansas Geological Survey
Open-file Report

Disclaimer

The Kansas Geological Survey does not guarantee this document to be free from errors or inaccuracies and disclaims any responsibility or liability for interpretations based on data used in the production of this document or decisions based thereon. This report is intended to make results of research available at the earliest possible date, but is not intended to constitute final or formal publication.

Approximate Analysis of Groundwater Mineralization Due to Discontinuity in an Impermeable Layer
Part 2: Seepage of Saltwater through a Semiconfining Discontinuity

Hillel Rubin* and Robert W. Buddemeier
Kansas Geological Survey, The University of Kansas
Lawrence, KS 66047

Kansas Geological Survey Open File Report 98-32

Approximate Analysis of Groundwater Mineralization Due to Discontinuity in an Impermeable Layer
Part 2: Seepage of Saltwater through a Semiconfining Discontinuity

Hillel Rubin* and Robert W. Buddemeier
Kansas Geological Survey, The University of Kansas
Lawrence, KS 66047

Abstract

This is the second report in a series of studies of groundwater mineralization in the Great Bend Prairie aquifer of Kansas by saltwater originating from a deeper Permian bedrock formation. Part 1 of this study addressed mineralization processes caused by direct contact between fresh and saltwater along local discontinuities in an impermeable layer that separates the freshwater aquifer from deep saltwater. However, field studies indicate that in various places the impermeable layer discontinuities expose subcrops of sandstone strata, which represent semipermeable strata within a matrix of low permeability siltstone layers. These exposed strata function as sources of saltwater seepage. This phenomenon is very similar to transmission of fluid through a semi-confining layer, in response to a local head differential. We have used this conceptual analogue as a basis for developing a simplified method for the simulation of salinity penetration through the discontinuity, and of the horizontal migration of the salinity to regions in the originally freshwater aquifer which are completely separated from the deep saltwater. Along the horizontal extent of the aquifer we have identified several regions. In all of them various types of regions of interest (ROI) were identified and top specified boundary layer (TSBL) simulations were applied.

The method developed in this paper can be useful as a simple but robust approach for the initial quantitative evaluation of mineralization processes typical of local semiconfining discontinuities in an impermeable layer separating a freshwater aquifer from a deep saltwater formation.

*On leave from the Department of Civil Engineering, Technion—Israel Institute of Technology, Haifa 32000, Israel.

Introduction

The general background of the research is given in part 1 of this study (Rubin and Buddemeier, 1998c), which for convenience will hereafter be referred to as report 1. In this report, only a brief outline relevant to the topic of this article is provided.

The studies covered by this report and report 1 originated from recent field observations and measurements (Buddemeier et al., 1994) as well as quantitative preliminary calculations based on previous studies of the authors (Rubin and Buddemeier, 1996, 1998a, b). These recent studies have indicated that mineralization processes of the Great Bend Prairie aquifer of south central Kansas might originate from local discontinuities in the impermeable layer that separates the freshwater aquifer from the deep Permian formation, which is saturated with saltwater. In western Kansas, that separation is provided by the Dakota formation which ends in central Kansas beneath the Great Bend Prairie aquifer but in south central Kansas, the impermeable layer discontinuities may lead to direct contact between fresh and saltwater along local exposures as discussed in report 1. In most cases, information gathered by Macfarlane et al. (1993), points to a conceptual approach considers the impermeable layer as the Permian siltstones. Discontinuities may be represented as comparatively thin oblique subcrops of sandstone layers which convey seeping saltwater from the deep Permian formation into the freshwater aquifer.

Rubin and Buddemeier (1998b) analyzed phenomena of groundwater mineralization due to continuous upward seepage of saltwater through a semiconfining barrier. This report improves the method of calculation of the salinity intrusion due to seepage and applies the method of report 1 to calculating the horizontal migration of the salinity to regions completely separated from the underlying saltwater.

The Conceptual Model and Basic Formulation

The simplified conceptual model shown in Fig. 1 describes a local discontinuity in an impermeable layer. This discontinuity allows seepage of saltwater from the zone of comparatively high head, existing in the deep formation, into the region of lower head in the freshwater aquifer. The length of the discontinuity is x_e^*. A Cartesian coordinate system is adopted, with the x^* axis representing the horizontal longitudinal direction and the y^* axis representing the vertical direction. The coordinate system origin is located at the upstream boundary of the impermeable layer discontinuity.

Flow conditions and salinity transport in the complete domain of Fig. 1 are governed by the following set of differential equations

$$\vec{q} = \frac{k}{\mu}(\nabla p - \rho \vec{g}) \tag{1}$$

$$\frac{\partial C^*}{\partial t^*} + \vec{V} \cdot \nabla C^* = \nabla \cdot \left(\tilde{D} \cdot \nabla^*\right) \tag{2}$$

where $\vec{q}$ is the specific discharge vector; k is the permeability; μ is the fluid density; g is the gravitational acceleration; C^* is the salt concentration (salinity); $\vec{V}$ is the interstitial flow velocity; $\tilde{D}$ is the dispersion tensor; t^* is the time.

Equations (1) and (2) represent a system of differential equations which can be solved by various types of numerical procedures. A major difficulty in such solutions is the nonlinearity stemming from the dependence of ρ on the value of C^*. However, in the domain of Fig. 1 this effect may be neglected, as the vertical component of the velocity is every where small. Furthermore, the salinity effect on the fluid density suppresses the vertical advection of the fluid particles. Therefore, neglect of the dependence of ρ on C* is a conservative approach with regard to salinity migration in the domain. The simplified forms of eqs. (1) and (2) are:

$$u = -\frac{\partial \Phi}{\partial x}; v = -\frac{\partial \Phi}{\partial y}; \nabla^2 \Phi = 0 \tag{3}$$

$$\frac{\partial C}{\partial t} + u\frac{\partial C}{\partial x} + v\frac{\partial C}{\partial y} = a_L \frac{\partial^2 C}{\partial x^2} + a\frac{\partial^2 C}{\partial y^2} \tag{4}$$

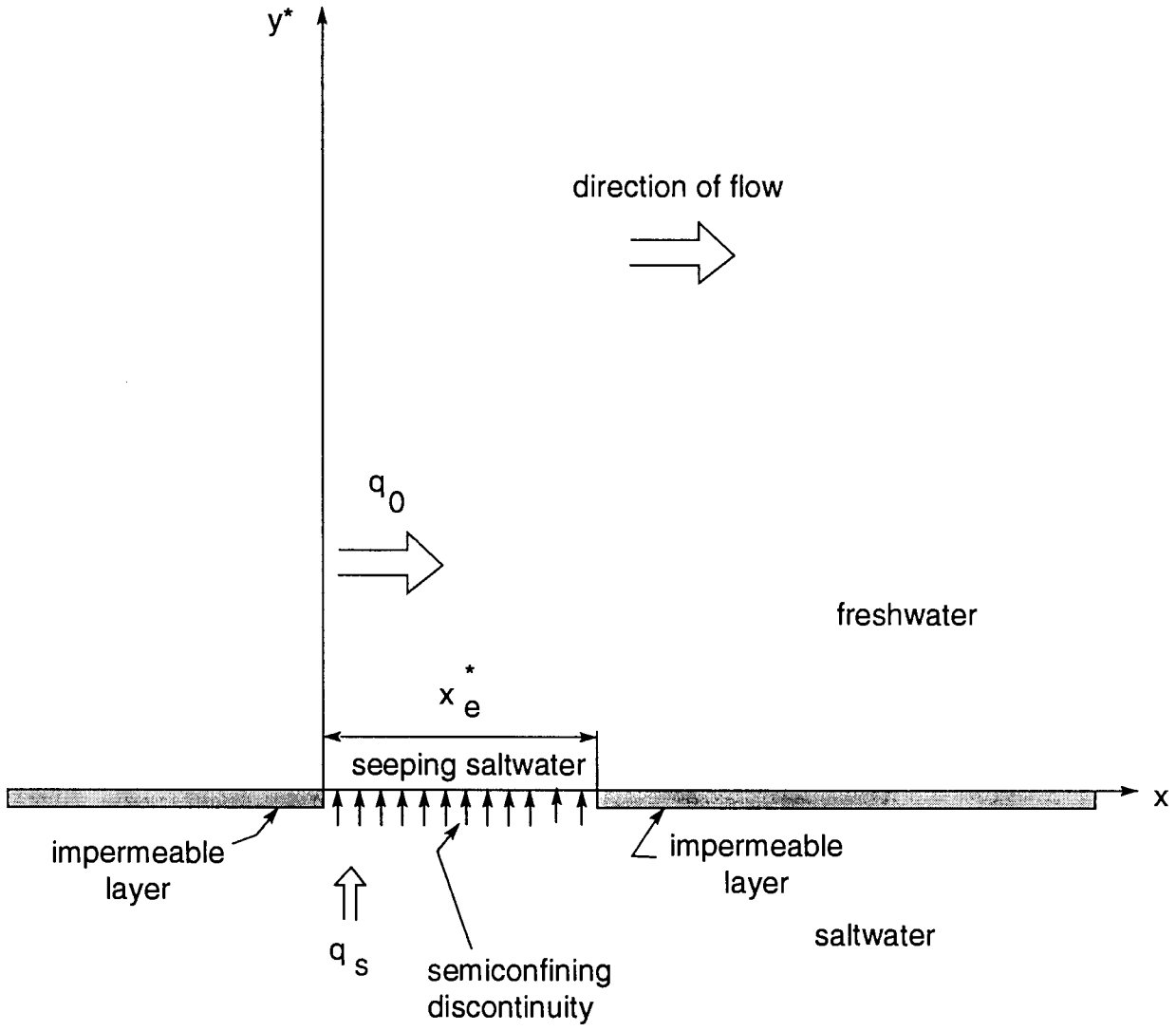

Fig. 1 Conceptual model representing the local semiconfining discontinuity in the impermeable layer and the region affected by the saltwater seepage.

where

$$x = x^* / l_0; y = y / l_0; u = U / U_0; v = V / U_0$$

$$\Phi = \frac{kg\rho_f}{\mu\phi l_0}\left(\frac{p}{\rho_f g} + y^*\right); t = t^* U_0 / l_0; C = \left(C^* - C_f^*\right) / \left(C_s^* - C_f^*\right)$$

$$a_L = D_x / \left(U_0 l_0\right); a = D_y / \left(U_0 l_0\right) \tag{5}$$

Here x^* and y^* are the longitudinal and vertical coordinates, respectively; U and V are horizontal and vertical components of the interstitial flow velocity, respectively; U_0 is the longitudinal flow velocity at the entrance cross section $x = 0$; D_x and D_y are the longitudinal and vertical components of the dispersion tensor; a_L and a are the dimensionless longitudinal and transverse dispersivities, respectively; l_0 is an arbitrary characteristic length; ϕ is the porosity; ρ_f is the density of the freshwater; and C_f^* and C_s^* are the fresh and saltwater salinities, respectively. The formulation of eq. (4) was based on the assumption that the vertical seepage velocity was much smaller than the flow induced by the horizontal hydraulic gradient.

To describe the flow in the domain of Fig. 1, we applied eq. (3) subject to the following boundary conditions:

$$\Phi = \Phi(x, y), \; x, y \geq 0$$

$$\Phi = 0; u = 1; v = 0 \quad at \quad x = 0$$

$$-\frac{\partial \Phi}{\partial x} = 1 + q_R x_e / y_{\max} \quad at \quad x = x_{\max} \quad \left(x_{\max} > x_e\right)$$

$$-\frac{\partial \Phi}{\partial y} = q_R \quad at \quad y = 0, \; 0 \leq x \leq x_e$$

$$-\frac{\partial \Phi}{\partial y} = 0 \quad at \quad y = 0, \; x_e < x \leq x_{\max}$$

$$-\frac{\partial \Phi}{\partial y} = 0 \quad at \quad y = y_{\max} \tag{6}$$

where x_{max} and y_{max} were the longitudinal and vertical extents of the simulated domain, respectively; q_R is the relative seepage discharge

$$q_R = q_s / q_0; q_0 = U_0 \phi \tag{7}$$

Here q_S is the specific (vertical) discharge of the seeping saltwater and q_0 is the specific discharge of the freshwater at $x = 0$.

With regard to the transport model of eq. (4) we considered the following initial and boundary conditions

$$
\begin{aligned}
&C = C(x,y,t),\ x,y,t \geq 0 \\
&C = 0 \quad at\ t = 0 \\
&C = 0 \quad at\ x = 0 \\
&C = 0 \quad at\ y = y_{\max} \\
&\frac{\partial C}{\partial x} \to 0 \quad at\ x = x_{\max} \\
&-a\frac{\partial C}{\partial y} = q_R(1-C) \quad at\ y = 0,\ 0 \leq x \leq x_e \\
&\frac{\partial C}{\partial y} = 0 \quad at\ y = 0,\ x_e < x \leq x_{\max}
\end{aligned}
\tag{8}
$$

Rubin and Buddemeier (1998b) developed a top specified boundary layer (TSBL) approach which modified the boundary condition of eq. (8) which referred to $y = 0$, where $0 \leq x \leq x_e$. The present study improves the accuracy of the calculation by conserving the essence of this boundary condition. Boundary layer (BL) simulations are compared with numerical simulations based on eqs. (3)–(8).

The Numerical Modeling

The discontinuity in the impermeable layer was represented by a semiconfining portion of length x_e. It could be represented as a salinity line source of contaminant, provided that the penetrating saline water flux was much smaller than the fresh aquifer specific discharge, and therefore did not affect flow conditions in the aquifer. At large distances downstream from the discontinuity, the short line source could be considered as a point source with strength equal to the total flux of salinity penetrating into the aquifer. Then by using the image method (e.g. Fischer et al., 1979), the impermeable layer could be simulated. It is also possible to apply power series solutions of

analogous heat conduction problems (Carslaw and Jaeger, 1959) to provide approximate solutions for the effects of salt water seeping into the fresh water aquifer. However, we have preferred to apply numerical simulations of the flow and contaminant transport in the aquifer in order to consider individually the quantitative significance of each of the approximations applied to the development of the boundary layer (BL) approach.

Report 1 showed that unsteady state conditions prevailed only in a comparatively small part of the domain containing the penetrating salinity front; this was called the "spearhead region." Therefore, all comparisons to numerical simulations referred only to the steady state region, located upstream of the spearhead region. In order to speed up the numerical simulations, we divided the domain into two sections. The first section included the impermeable layer discontinuity and a small portion of the domain downstream of that discontinuity. In this section of the domain, there were some vertical flows induced by the saltwater, which seeped into the domain. The second section of the domain was essentially subject to horizontal flow only, and vertical components of the velocity were negligible. We might consider that in the second section of the domain the velocity was uniformly distributed. Under such conditions there was no need to solve the Laplace equation of flow in the second section.

Steady state conditions of flow were assumed for the velocity distribution in the first section of the domain. Then by applying a finite difference approximation of eq. (3), the following successive over-relaxation (SOR) procedure for the determination of the dimensionless potential function Φ was obtained:

$$\Phi_{i,j}^{(n+1)} = (1-\omega)\Phi_{i,j}^{(n)} + \omega\left[\beta_1\left(\Phi_{i-1,j}^{(n)} + \Phi_{i+1,j}^{(n)}\right) + \beta_2\left(\Phi_{i,j-1}^{(n+1)} + \Phi_{i,j+1}^{(n)}\right)\right], \qquad (9)$$

where i and j refer to nodal point numbers in the longitudinal and vertical directions, respectively; ω is the over-relaxation parameter; (n) is the number of the iteration. The coefficients β_1 and β_2 of eq. (9) are given as

$$\beta_0 = 2\left[1+\left(\frac{\Delta x}{\Delta y}\right)^2\right];\ \beta_1 = 1/\beta_0;\ \beta_2 = \left(\frac{\Delta x}{\Delta y}\right)^2 / \beta_0 \tag{10}$$

where Δx and Δy are the longitudinal and vertical intervals, respectively.

The numerical scheme of eq. (9) was associated with the appropriate presentation of the boundary conditions given by eq. (6). Convergence of the SOR iteration procedure of eq. (9) was guaranteed as the dominant coefficients of the system of linear equations represented by eq. (9) formed the diagonal of the coefficient matrix.

With regard to the contaminant transport in the domain, we applied two types of finite difference schemes to eq. (4). We applied again an SOR iterative scheme to the determination of the salinity distribution in the domain while considering all terms of eq. (4), subject to steady state. This type of iterative scheme is given as

$$C_{i,j}^{(n+1)} = (1-\omega)C_{i,j}^{(n)} + \omega\left(\gamma_1 C_{i-1,j}^{(n+1)} + \gamma_2 C_{i+1,j}^{(n)} + \gamma_3 C_{i,j-1}^{(n+1)} + \gamma_4 C_{i,j+1}^{(n)}\right) \tag{11}$$

where

$$\begin{aligned}
\gamma_0 &= \frac{u_{i,j}}{\Delta x} + \frac{v_{i,j}}{\Delta y} + \frac{2a_L}{(\Delta x)^2} + \frac{2a}{(\Delta y)^2} \\
\gamma_1 &= \left[\frac{u_{i,j}}{\Delta x} + \frac{a_L}{(\Delta x)^2}\right] / \gamma_0;\ \gamma_2 = \left[\frac{a_L}{[\Delta x]^2}\right] / \gamma_0 \\
\gamma_3 &= \left[\frac{v_{i,j}}{\Delta y} + \frac{a}{(\Delta y)^2}\right] / \gamma_0;\ \gamma_4 = \left[\frac{a}{(\Delta y)^2}\right] / \gamma_0
\end{aligned} \tag{12}$$

The usage of the SOR scheme of eq. (11) was, however, very inconvenient for a long, narrow domain in which Δy was considerably smaller than Δx. For the particular cases of interest to this study we found that the effect of longitudinal dispersion was very minor and could be neglected. Therefore eq. (14) was approximated as

$$u\frac{\partial C}{\partial x} + v\frac{\partial C}{\partial y} = a\frac{\partial^2 C}{\partial y^2} \tag{13}$$

Also, the boundary condition at $x \to \infty$ was not required. Therefore, eq. (13) is analogous to a time dependent one-dimensional contaminant transport problem, in which the x-coordinate replaces the time coordinate.

We applied a backward finite difference approximation of the second left-hand side term of eq. (13) and a Crank-Nicolson approximation of the right hand term of this equation to obtain

$$-\alpha_1 C_{i,j-1} + \alpha_2 C_{i,j} - \alpha_3 C_{i,j+1} = \alpha_4 \tag{14}$$

where

$$\alpha_1 = \frac{v_{i,j}}{\Delta y} + \frac{a}{2(\Delta y)^2};\ \alpha_2 = \frac{u_{i,j}}{\Delta x} + \frac{v_{i,j}}{\Delta y} + \frac{a}{(\Delta y)^2}$$

$$\alpha_3 = \frac{a}{2(\Delta y)^2};\ \alpha_4 = C_{i-1,j-1}\frac{a}{2(\Delta y)^2} + C_{i-1,j}\left[\frac{u_{i,j}}{\Delta x} - \frac{a}{(\Delta y)^2}\right] + C_{i-1,j+1}\frac{a}{2(\Delta y)^2} \tag{15}$$

Stability analysis by the procedure of von Neumann (e.g. Lapidus and Pinder, 1982) indicated that the numerical scheme of eq. (14) was unconditionally stable.

It is also possible to take a central finite difference approximation of the second left-hand side term of eq. (13). However, then the stability analysis indicates that such a scheme was applicable provided that the following relationship was satisfied:

$$\frac{2}{\Delta y} \geq \frac{q_R}{a} \tag{16}$$

Application of the Top Specified Boundary Layer (TSBL)

Figure 2 shows the various types of BLs considered by the present study. The major objective of the calculation was to determine the thickness δ of the region of interest (ROI) which is defined as a TSBL, namely at the top of the ROI $y = \delta$ and $C = C_T$, where C_T is the acceptable value of C. All our calculations considered $C_T = 0.01$.

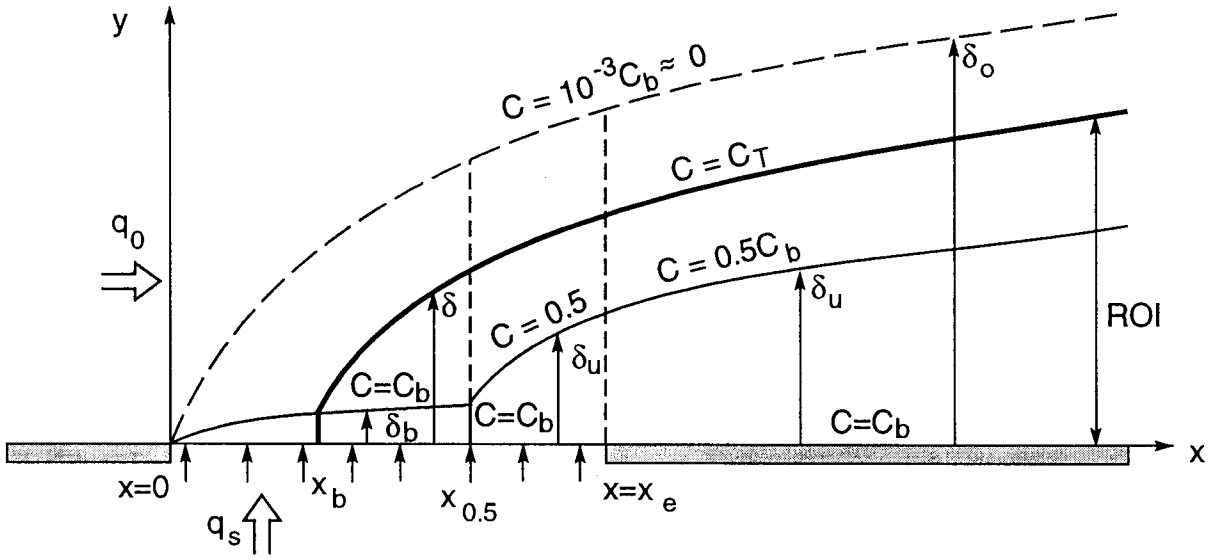

Fig. 2 Regions and zones identifying the various BLs at the impermeable layer discontinuity and downstream.

We identified in the domain three different ranges of x values, which defined three different sections in the domain. Each section was characterized by a different set of BLs. The different sections were defined according to the following ranges of x-values.

$$0 \le x \le x_{0.5}$$
$$x_{0.5} \le x \le x_e$$
$$x_e \le x \qquad (17)$$

where $x_{0.5}$ was the value of x, at which the bottom salinity value C_b reached the steady state value of 0.5.

In the entire domain, vertical flow velocities were considered small enough to be negligible. We also ignored effects of longitudinal dispersion in the entire domain. If the thickness of the domain was large and $q_R << 1$, we also neglected the effect of the seeping saltwater on the aquifer flow. The last assumption was not essential, but considerably simplified the calculation. The neglect of the vertical velocities in the entire domain created some difficulty with regard to the boundary condition of eq. (8) referring to $y = 0$, $0 \le x \le x_e$. Rubin and Buddemeier (1998b) overcame that difficulty by introducing a modification into the boundary condition. This modification magnified the predictions of salinity penetration into the freshwater aquifer. Therefore, the previous approach could be considered excessively conservative. In the present study some new concepts were introduced that allowed us to conserve the essence of the last boundary condition of eq. (8).

The following paragraphs devote separate discussions to each range of x-values represented in eq. (17).

Range of x-values $0 \le x \le x_{0.5}$

In this range of x-values we divided the domain into two regions as shown in Fig. 2. At the bottom of the originally freshwater aquifer we assumed that a region of almost uniform salinity distribution was subject to build-up at $0 \le y \le \delta_b$. This region was termed as the bottom BL, in

which the salinity value was C_b. On top of the bottom BL, at $\delta_b \le y \le \delta_o$, the salinity varied between C_b and $10^{-3}C_b$. This region was called the outer BL. At the top of the outer BL the salinity practically vanished (i.e., it was smaller than the acceptable value, C_T, by at least an order of magnitude).

As illustrated in the left-hand side of Fig. 3, conservation of mass with regard to vertical transport affecting the bottom BL yielded:

$$\frac{d}{dt}(C_b\delta_b) = q_R C_b \tag{18}$$

where

$$\frac{d}{dt} = \frac{\partial}{\partial t} + \frac{\partial}{\partial x} \tag{19}$$

In the outer BL we assumed the following salinity profile

$$C = C_b L(\eta);\ \eta = \frac{y-\delta_b}{\delta_0 - \delta_b};\ \delta_b \le y \le \delta_0 \tag{20}$$

The function $L(\eta)$ was represented as a power series by

$$L = (1-\eta)^n \tag{21}$$

where n is a power coefficient. The value of n should be determined by comparison of calculated salinity profiles to measured ones, or to results obtained by accurate simulations.

According to Fig. 3 consideration of mass conservation at the outer BL yielded:

$$\frac{d}{dt}\left[(\delta_0 - \delta_b)C_b\right] = -\frac{aL'(0)C_b}{(\delta_0 - \delta_b)\int_0^1 L d\eta} \tag{22}$$

Reference to the boundary conditions of eq. (8) implied:

$$-\frac{aL'(0)C_b}{\delta_0 - \delta_b} = q_R(1 - C_b) \tag{23}$$

Considering eq. (21) the following quantities were obtained

$$L'(0) = -n;\ \int_0^1 L d\eta = 1/(n+1) \tag{24}$$

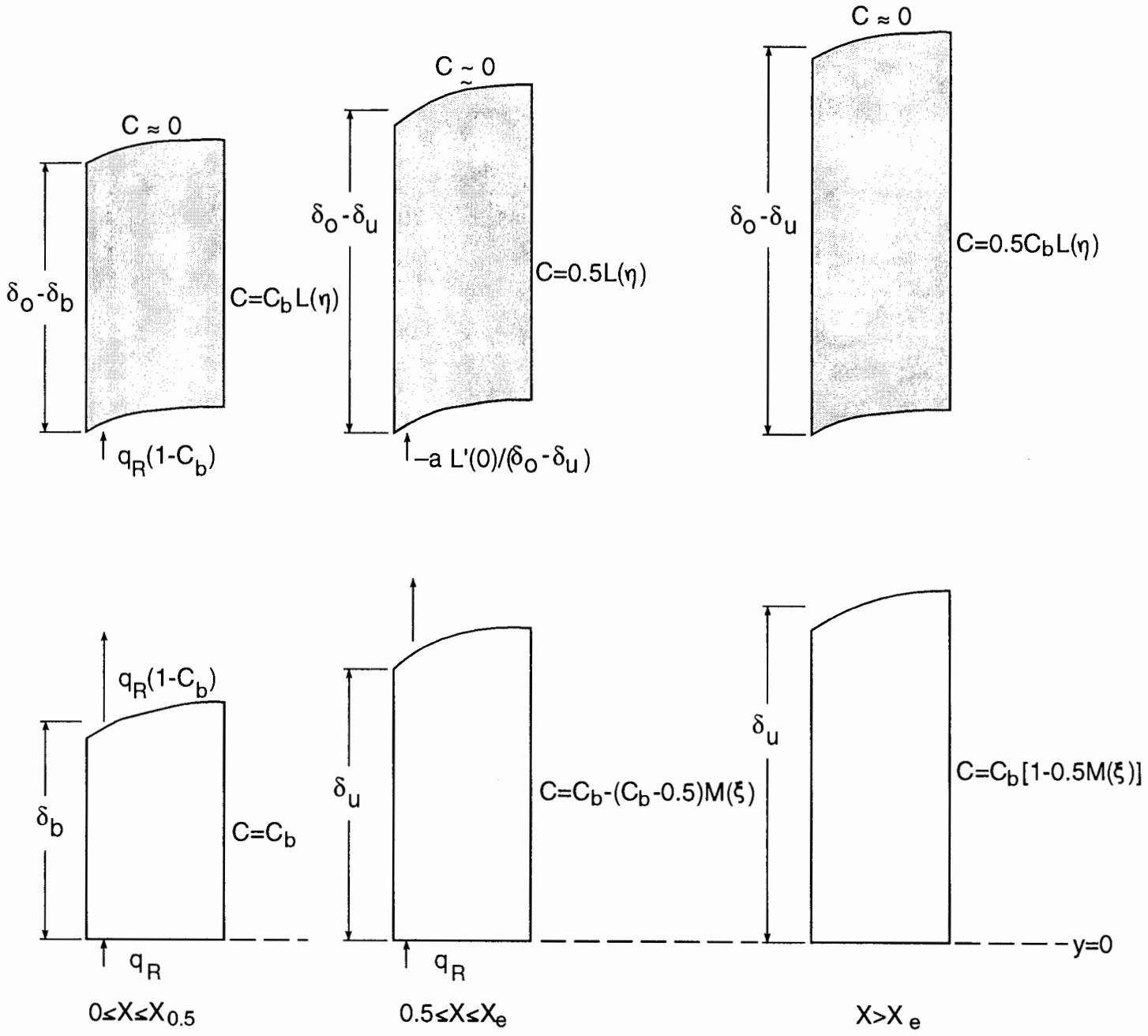

Fig. 3 Definitions of BL thickness, distributions of salinity, and vertical fluxes of salinity for the various BLs associated with the ranges of x values shown in Fig. 2.

It was convenient to apply the modified coordinate τ to the presentation of the various domain variables. The definition and range of application of τ are

$$\tau = \delta_0 - \delta_b;\ 0 \le \tau \le an / q_R \tag{25}$$

Some expansion and a different presentation of eq. (22) applied to eq. (25) yielded:

$$\tau \frac{d\tau}{dt} + \tau^2 \frac{d}{dt}(\ln C_b) = an(n+1) \tag{26}$$

By introducing eq. (24) into eq. (23), we obtained:

$$C_b = \frac{\tau}{\tau + an / q_R} \tag{27}$$

According to eqs. (25) and (27), the range of C_b values is given by:

$$0 \le C_b \le 0.5 \tag{28}$$

Introducing eq. (27) into eq. (26) we obtained

$$\frac{d\tau}{dt} = an(n+1)G(\tau) \tag{29}$$

where

$$G(\tau) = \frac{\tau + an / q_R}{\tau(\tau + 2an / q_R)} \tag{30}$$

Direct integration of eq. (29) and reference to the initial condition of t, $x = 0$ at $\tau = 0$ yielded

$$\begin{aligned} x &= \frac{1}{an(n+1)} H(\tau) \quad if \quad 0 \le x \le x_{0.5}, t \\ t &= \frac{1}{an(n+1)} H(\tau) \quad if \quad t \le x \le x_{0.5} \end{aligned} \tag{31}$$

where

$$H(\tau) = \frac{1}{2}\tau^2 + \frac{an}{q_R}\tau - \left(\frac{an}{q_R}\right)^2 \ln\left(1 + \tau \frac{q_R}{an}\right) \tag{32}$$

As indicated by eq. (25) the variable τ obtains its maximum value at $x_{0.5}$. We introduced this relationship into eqs. (31) and (32) to obtain:

$$x_{0.5} = \frac{an}{q_R^2(n+1)}\left[\frac{3}{2} - \ln(2)\right] \approx 0.8\frac{an}{q_R^2(n+1)} \tag{33}$$

According to eq. (31) the part of the domain represented by the range of x-values $0 \le x \le x_{0.5}$, or identically by the range of τ values given by eq. (25), is subject to steady state conditions at $t \ge x_{0.5}$.

Following the determination of $x(\tau)$, or $t(\tau)$, according to eq. (31), and $C_b(\tau)$ according to eq. (27), a closed form analytical representation was developed for $\delta_b(\tau)$ as shown in the following paragraph.

According to eq. (18):

$$C_b\delta_b = q_R\int C_b dt \tag{34}$$

We applied eq. (31), to represent dt by $d\tau$, and obtained:

$$dt = \frac{d\tau}{an(n+1)}\left[\tau + \frac{an}{q_R}\left(\frac{\tau}{\tau + an/q_R}\right)\right] \tag{35}$$

Introducing eqs. (27) and (35) into eq. (34) and performing the integration while considering that at $t = 0$, the left hand side of eq. (34) vanished, we obtained:

$$C_b\delta_b = \frac{q_R}{an(n+1)}\left[\frac{1}{2}\tau^2 + \left(\frac{an}{q_R}\right)^2 - \left(\frac{an}{q_R}\right)^3\left(\frac{1}{\tau + an/q_R}\right) - \left(\frac{an}{q_R}\right)^2 \ln\left(1 + \tau\frac{q_R}{an}\right)\right] \tag{36}$$

Equations (27) and (36) provided complete information about values of C_b and δ_b.

At the upper limit of τ, namely at $x = x_{0.5}$, provided that $t > x_{0.5}$, eq. (36) yielded:

$$(\delta_b)_{x=x_{0.5}} \approx \frac{0.61an}{q_R(n+1)} \tag{37}$$

or, by applying eq. (25):

$$(\delta_b)_{x=x_{0.5}} \approx \frac{0.61}{n+1.61}(\delta_0)_{x=x_{0.5}} \tag{38}$$

The region of interest (ROI) was defined as the region in which the value of C exceeded the acceptable value, C_T. Therefore, according to eqs. (20) and (21):

$$\eta_T = 1-(C_T / C_b)^{1/n} \tag{39}$$

where η_T is the value of η at the top of the ROI.

The ROI vanished as long as C_b was smaller than the acceptable value C_T. The build-up of the ROI was performed downstream of $x = x_b$ where at x_b the value of C_b was equal to C_T. According to eq. (27):

$$\tau_b = C_T \frac{an}{q_R(1-C_T)} \approx C_T \frac{an}{q_R} \tag{40}$$

where τ_b is the value of τ at x_b.

Introducing eq. (40) into eq. (32) we obtained:

$$H(\tau_b) \approx C_T\left(\frac{an}{q_R}\right)^2 = \frac{\tau_b^2}{C_T} \tag{41}$$

Introducing this expression into eq. (31) we obtained:

$$x_b = \frac{anC_T}{q_R^2(n+1)} \tag{42}$$

Introducing values of τ_b from eq. (40) into eqs. (30 and (36) we obtained:

$$G(\tau_b) \approx \frac{q_R}{2anC_T} \tag{43}$$

$$\delta_b(\tau_b) = \delta(\tau_b) \approx \frac{anC_T}{2(n+1)q_R} \tag{44}$$

Downstream of $x = x_b$ the thickness of the ROI according to eqs. (27) and (39) is given by:

$$\delta = \delta_b + \tau - \tau^{1-1/n}\left[C_T(\tau + an / q_R)\right]^{1/n} \tag{45}$$

The method of approximation applied over the range of $0 \le x \le x_{0.5}$ could be applied to the complete range of $0 \le x \le x_e$. However, the numerical simulations showed that the salinity

gradient at the bottom of the aquifer substantially decreased when $C_b \rightarrow 1$. Therefore, to allow better matching of salinity profiles at $x = x_e$ as well as higher accuracy we developed another approximation method for the range $0 \le x \le x_e$ as shown in the following section.

Range of x-values $x_{0.5} \le x \le x_e$

In this range of x-values we divided the domain into two regions as shown in Fig. 2. At the bottom of the originally freshwater aquifer we consider that an inner BL was subject to build-up at $0 \le y \le \delta_u$. The salinity in this region varied between $C = C_b$ and $C = 0.5$. On top of the inner BL, the outer BL was built-up at $\delta_u \le y \le \delta_0$. The salinity in this region varied between $C = 0.5$ and a negligible value, which we defined as salinity smaller than C_T by at least an order of magnitude.

In the inner BL we assumed the following salinity profile:

$$C = C_b - (C_b - 0.5)M(\xi);\ \xi = \frac{\delta_u - y}{\delta_u};\ 0 \le y \le \delta_u \tag{46}$$

where $M(\xi)$ was represented as a power series:

$$M = (1-\xi)^{n_1} \tag{47}$$

where n_1 is a power coefficient whose value should be determined by comparison of calculated salinity profiles to measured values.

According to Fig. 3, combination of mass conservation in the inner BL with eq. (46) yielded:

$$\frac{d}{dt}\left[\delta_u \frac{n_1 C_b + 0.5}{n_1 + 1}\right] = q_R - \frac{(C_b - 0.5)n_1}{\delta_u} \tag{48}$$

In the outer BL we assumed the following salinity profile:

$$C = 0.5L(\eta);\ \eta = \frac{y - \delta_u}{\delta_0 - \delta_u};\ \delta_u \le y \le \delta_0 \tag{49}$$

The function L was represented by

$$L = (1-\eta)^{n_2} \tag{50}$$

As illustrated in Fig. 3, combination of mass conservation in the outer BL with eq. (50) yielded:

$$\frac{d}{dt}\left[(\delta_0 - \delta_u)\right] = \frac{an_2(n_2+1)}{\delta_0 - \delta_u} \tag{51}$$

Continuity of the salinity profile at $y = \delta_u$ yielded:

$$\frac{(C_b - 0.5)n_1}{\delta_u} = \frac{n_2}{\delta_0 - \delta_u} \tag{52}$$

Rearrangement of terms yielded:

$$C_b = 0.5\left[1 + \frac{n_2}{n_1}\frac{\delta_u}{\delta_0 - \delta_u}\right] \tag{53}$$

For comparatively large values of x the value of C_b approached unity, then

$$\frac{\delta_0}{\delta_u} \rightarrow \frac{n_1}{n_2} + 1 \tag{54}$$

The build-up of the regions of inner and outer BLs started at $t = x_{0.5}$. The characteristics of these BLs were given by eqs. (46) and (49). The following expressions apply to values of $x <$ t. For x-values larger than t, the parameter t should be inserted instead of x. In such a manner we avoided writing long expressions incorporating the step function.

Direct integration of eq. (51) yielded:

$$(\delta_0 - \delta_u)^2 = 2an_2(n_2+1)(x - x_{0.5}) + (\delta_0 - \delta_u)^2_{x=x_{0.5}} \tag{55}$$

It is convenient and very reasonable to assume

$$(\delta_0 - \delta_u)_{x=x_{0.5}} = (\delta_0 - \delta_b)_{x=x_{0.5}} \tag{56}$$

$$(\delta_u)_{x=x_{0.5}} = (\delta_b)_{x=x_{0.5}} \tag{57}$$

These expressions are subject to minor modification to comply with mass conservation.

We introduced eqs. (52) and (55) into eq. (48) and performed a direct integration to obtain:

$$\delta_u \frac{n_1 C_b + 0.5}{n_1 + 1} = q_R(x - x_{0.5}) - \frac{1}{2(n_2+1)}\left[2an_2(n_2+1)(x - x_{0.5}) + (\delta_0 - \delta_u)^2_{x=x_{0.5}}\right]^{0.5} + \frac{1}{2(n_2+1)}(\delta_0 - \delta_u)_{x=x_{0.5}} + \frac{1}{2}(\delta_u)_{x=x_{0.5}} \quad (58)$$

Introducing eq. (53) into eq. (58) we obtained:

$$\delta_u = \frac{(n_1+1)(\delta_0 - \delta_u)}{2n_2}\left[(1+F)^{0.5} - 1\right] \quad (59)$$

where

$$F = \frac{8\, fn_2}{(n_1+1)(\delta_0 - \delta_u)} \quad (60)$$

$$f = q_R(x - x_{0.5}) - \frac{1}{2(n_2+1)}(\delta_0 - \delta_u) + \frac{1}{2(n_2+1)}(\delta_0 - \delta_u)_{x=x_{0.5}} + \frac{1}{2}(\delta_u)_{x=x_{0.5}} \quad (61)$$

The top of the ROI was again defined by the isohaline $C = C_T$. Applying eq. (49) we obtained:

$$\eta_T = 1 - (2C_T)^{1/n_2} \quad (62)$$

$$\delta = \delta_u + (\delta_0 - \delta_u)\eta_T = \delta_0 \eta_T + (1 - \eta_T)\delta_u \quad (63)$$

Range of x-values $x > x_e$

For this range of x-values, we adopted the method developed in report 1. However, matching between the right- and left-hand side salinity profiles at $x = x_e$ was different, as C_b at the left hand side of x_e could be larger or smaller than 0.5. For the appropriate presentation of the present paper, only a brief review and general outline of this method are given here.

According to report 1, as shown in Figs. 2 and 3, the simulated domain incorporated an inner and an outer BL. There was no salinity transfer between these two BLs. Vertical salinity gradients only led to expansion of the BLs.

The salinity profile in the inner BL, which was adjacent to the aquifer bottom, was given by

$$C = C_b\left[1-(1-c_r)M(\xi)\right];\quad \xi = \frac{\delta_u - y}{\delta_u};\quad 0 \le y \le \delta_u \tag{64}$$

where

$$M = (1-\xi)^{n_3} \tag{65}$$

Here n_3 is a power coefficient which is not necessarily identical to n_1 of eq. (47); c_r was the ratio between the salinity at $y = \delta_u$ and the salinity C_b, at $y = 0$. In the course of numerical experiments (report 1), it was found most appropriate to consider $c_r = 0.5$. However, in the present study another set of experiments was needed to identify the most appropriate values of c_r relevant to the scope of the present study.

The outer BL was built-up on top of the inner BL. The salinity profile in the outer BL is given by

$$C = c_r C_b L(\eta);\quad \eta = \frac{y-\delta_u}{\delta_0 - \delta_u};\quad \delta_u \le y \le \delta_0 \tag{66}$$

where

$$L = (1-\eta)^{n_4} \tag{67}$$

Here n_4 is a power coefficient not necessarily identical to n_2 of eq. (50).

The salinity distribution at $x = x_e$ provided the boundary condition for salinity transport and distribution at $x > x_e$. At $t = x_e$ the salinity distribution at $x = x_e$ is subject to steady state conditions, as implied by calculations referring to $x < x_e$. At $x > t + x_e$ there was no salinity penetration. Upstream of $x = t + x_e$ values of the thickness of the inner and outer BLs are given respectively by:

$$\left(\delta_u^2\right)_x = \left(\delta_u^2\right)_{x_e} + \alpha_1 \frac{2a(1-c_r)n_1(n_1+1)}{n_1+c_r}(x-x_e) \tag{68}$$

$$(\delta_0 - \delta_u)_x^2 = (\delta_0 - \delta_u)_{x_e}^2 + 2\alpha_2 a n_2 (n_2+1)(x-x_e) \tag{69}$$

where $\alpha_1 = 0.935$, and $\alpha_2 = 0.775$.

The ratio between δ_0 and δ_u is given by eq. (54) with n_3 and n_4 replacing n_1 and n_2, respectively. If x_e is sufficiently large, then the value of C_b at x_e is about unity. Then, the inner and outer BLs at $x > x_e$ represent a direct extension of these layers at $x_{0.5} \leq x \leq x_e$, provided that $c_r = 0.5$. It should be noted that $c_r = 0.5$ was adopted in report 1 as the best-fit value in the case analyzed by that study. If C_b at x_e is significantly different from unity, then the best match of salinity profiles to calculated curves on both sides of $x = x_e$ should be determined.

According to report 1 the value of C_b was given by

$$(C_b)_{x,t} = (\delta_u C_b)_{x=x_e, t_e=t-x+x_e} / (\delta_u)_{x,t} \tag{70}$$

The ROI was again defined in this study as the region in which the salinity exceeded its acceptable value, C_T. The ROI was represented as a top specified boundary layer (TSBL) whose thickness was δ.

If $\delta_u < \delta < \delta_0$ then

$$\eta_T = 1 - \left(\frac{C_T}{c_r C_b}\right)^{1/n_4} \tag{71}$$

$$\delta = \eta_T \delta_0 + (1 - \eta_T)\delta_u \tag{72}$$

If $0 < \delta < \delta_u$ then

$$\xi_T = 1 - \left(\frac{1 - c_r / C_b}{1 - c_r}\right)^{1/n_3} \tag{73}$$

$$\delta = \delta_u (1 - \xi_T) \tag{74}$$

Preliminary Tests

Our preliminary tests concerned the possible employment of the BL method developed in this paper, and addressed its adequacy. The objective of the tests was also to determine possible basic parameters for the models developed for each range of x-values. The test results presented in the

following section address the complete determination of parameters and matching of salinity profiles at each boundary separating adjacent ranges of x-values.

Figures 4 and 5 show the distribution of the ratio between the thickness of δ_0 and of δ_u, which is defined as δ_R. This ratio was calculated at $0 \leq x \leq x_e$ only if C_b was larger than 0.5. At $0 \leq x \leq x_e$ the value of δ_u represented the isohaline $C = 0.5$. At $x \geq x_e$ the value of δ_u represents the normalized isohaline $C/C_b = 0.5$. Some very large values of δ_R have been omitted at $x_{0.5}$ in order to allow appropriate presentation of δ_R for the complete range of x-values.

For the complete range of q_R values considered in Fig. 4, the value of δ_R at $x \geq x_e$ approaches a constant value, $\delta_R \rightarrow 3.17$. This phenomenon also occurred in the case analyzed in report 1. Therefore, downstream of x_e, as shown in Fig. 4, the model developed in report 1 could basically be applied to the calculations of the present study. However, δ_R in proximity to x_e, acquired significantly different values for large and small values of a. In order to identify the cause of this phenomenon and to quantify its effect, we performed another set of numerical experiments whose results are depicted in Fig. 5. The experiments used the largest expected value of q_R, namely $q_R = 0.1$, and a comparatively large value of x_e, namely $x_e = 100$. Fig. 5 indicates that for very large values of q_R and very small values of a (i.e. very large values of q_R/a) the value of δ_R does not obtain its asymptotic value even at a very large distance downstream of x_e. Figs. 4 and 5 also indicate that for large values of q_R/a, the value of δ_R decreases with x upstream of x_e, and probably approaches a value of the order of magnitude of unity. However, in none of these figures was such an asymptotic value obtained, due to the comparatively short horizontal extent of the impermeable layer discontinuity.

We might conclude that in the range $x_{0.5} \leq x \leq x_e$ some difficulties in calibration of the BL model could be encountered. According to Fig. 5 we might also expect difficulties in applying the BL model at $x \geq x_e$ if q_R/a were very large.

Figure 6 represents results of numerical experiments to identify the best-fit value of n_3 and n_4. Besides determining the salinity profiles by numerical procedures, at each relevant cross section we considered values of n_4 and calculated the value of n_3 by applying the relationship

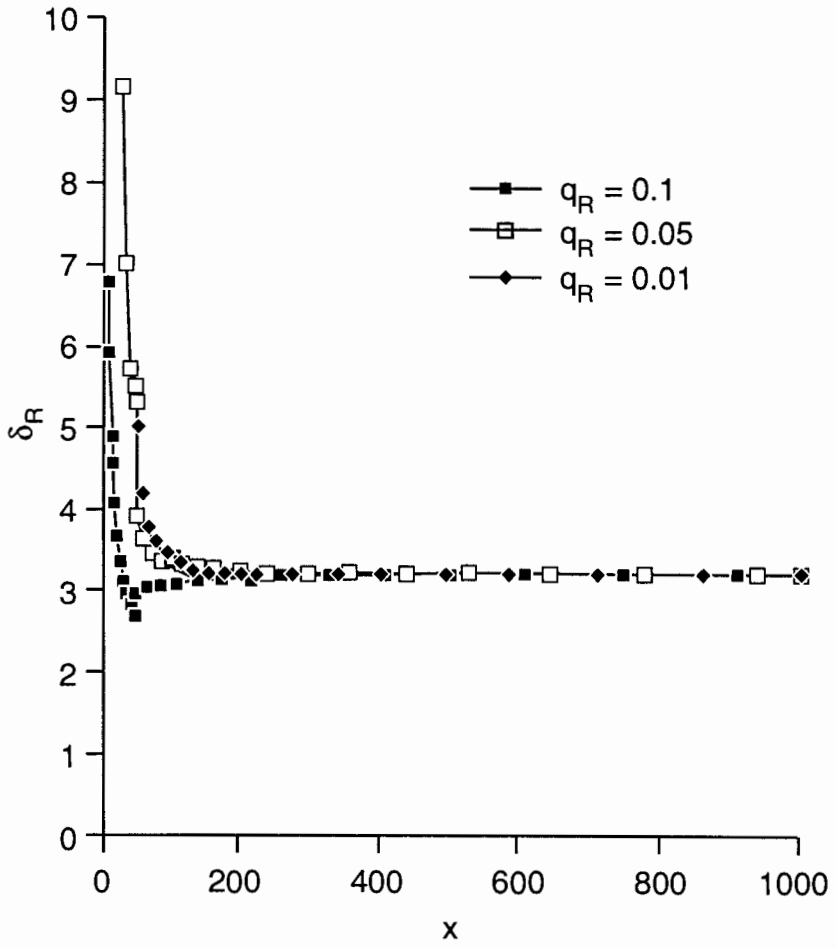

Fig. 4 Values of δ_R for various values of q_R ($a = 0.1$, $x_e = 50$).

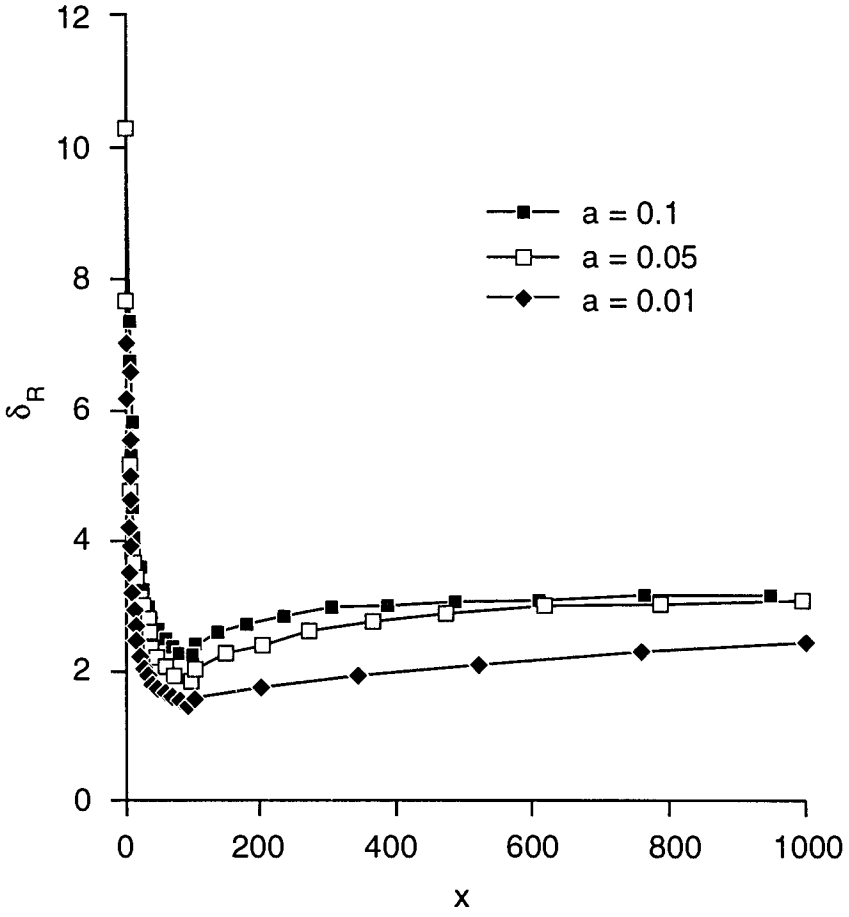

Fig. 5 Values of δ_R at high values of q_R/a for various values of a ($q_R = 0.1$, $x_e = 100$).

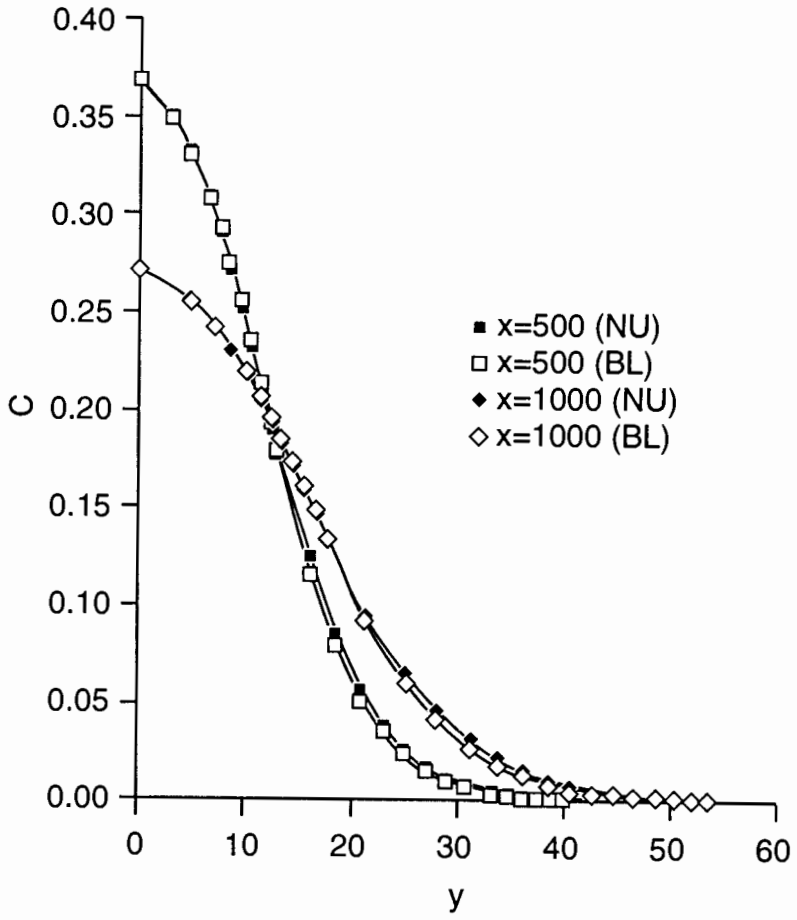

Fig. 6 Best fit between power series expansions and numerically calculated salinity profiles ($a = 0.1$, $q_R = 0.1$, $x_e = 50$, $n_4 = 4$).

$$n_3 = n_4 / (\delta_R - 1) \tag{75}$$

Fig. 6 shows that appropriate values of n_3 and n_4 were:

$$n_4 = 4; \quad n_3 = 1.84 \tag{76}$$

These values were identical to those found in report 1. However, they must be applied very carefully. At comparatively large values of x_e and q_R/a the seeping saltwater creates a "saltwater mound." Then the model at $x \geq x_e$ could not be rigorously applied. The "saltwater mound" phenomenon represents the build-up of a comparatively thick layer of water with very high salinity, in which salinity gradients are comparatively small. This phenomenon is magnified by large values of x_e and q_R/a, and introduces difficulties in applying the BL model developed in this study. However, cases of mineralization in the Great Bend Prairie aquifer do not often fall into the category of "saltwater mound" build-up.

Characterizing the Mineralization Process

Presentation of the mineralization process in terms of the BL characteristics has two major advantages:

(a) it provides basic information about the intensity of the mineralization process by applying a basic set of simple parameters, and

(b) it provides a simple and robust method for the quantification of the mineralization phenomenon.

The set of important basic parameters consisted mainly of values of δ and C_b. Parameters like δ_0, δ_u and the salinity profiles were of less importance. However, the complete presentation of the method required reference to all these parameters.

Very small values of q_R/a were considered for the range of x-values $0 \leq x \leq x_{0.5}$. Otherwise this range was very short. Fig. 7 provides a single example of our characterization procedure. By choosing $n = 3$ we obtained quite good agreement between the numerical and BL

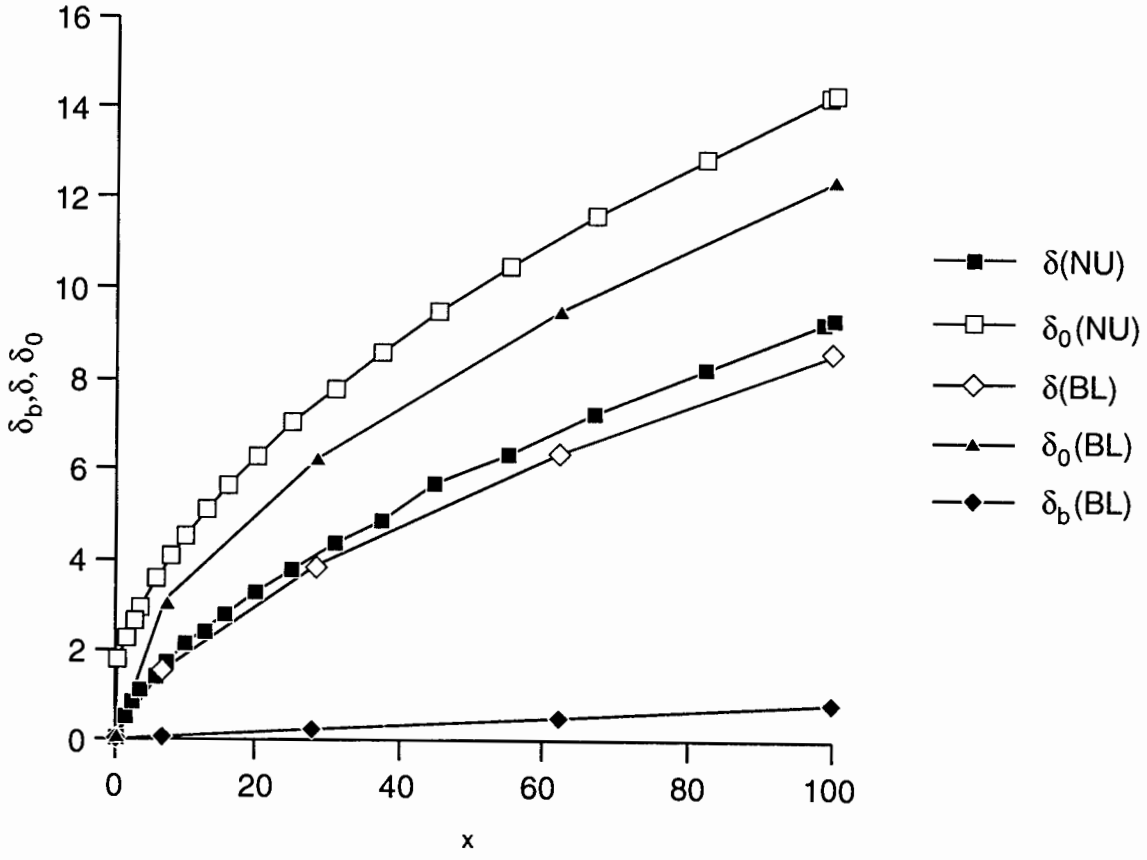

Fig. 7a Characteristics of the range $0 \leq x \leq x_{0.5}$ ($a = 0.1$, $q_R = 0.01$, $n = 3$)

(a) Values of δ_b, δ, δ_0

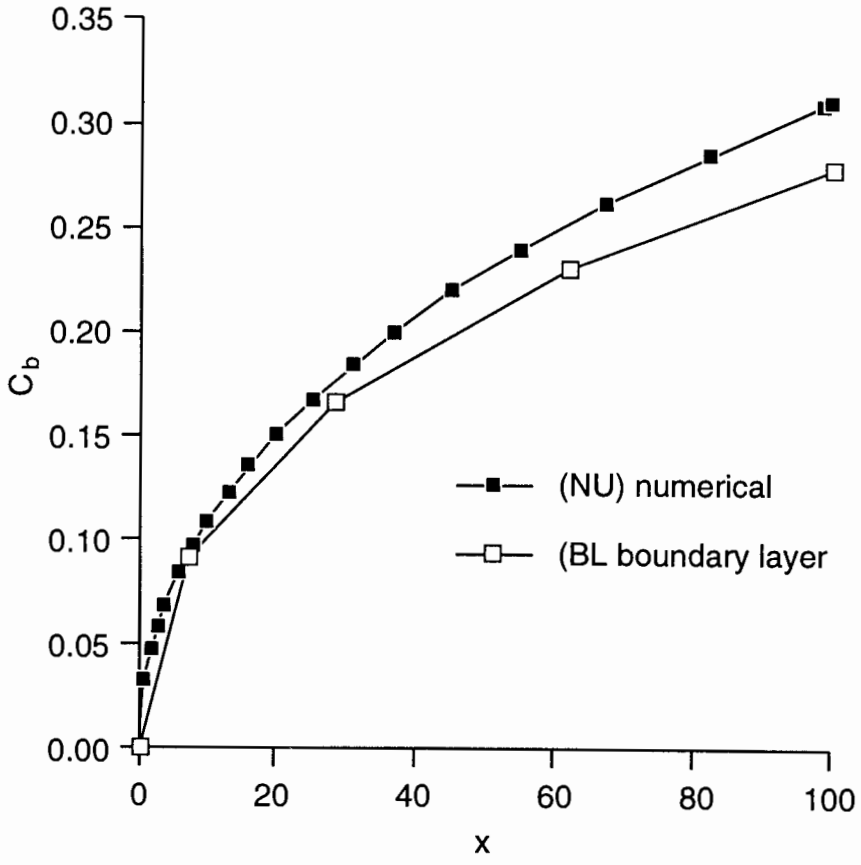

Fig. 7b Characteristics of the range $0 \leq x \leq x_{0.5}$ ($a = 0.1$, $q_R = 0.01$, $n = 3$)

(b) Values of C_b

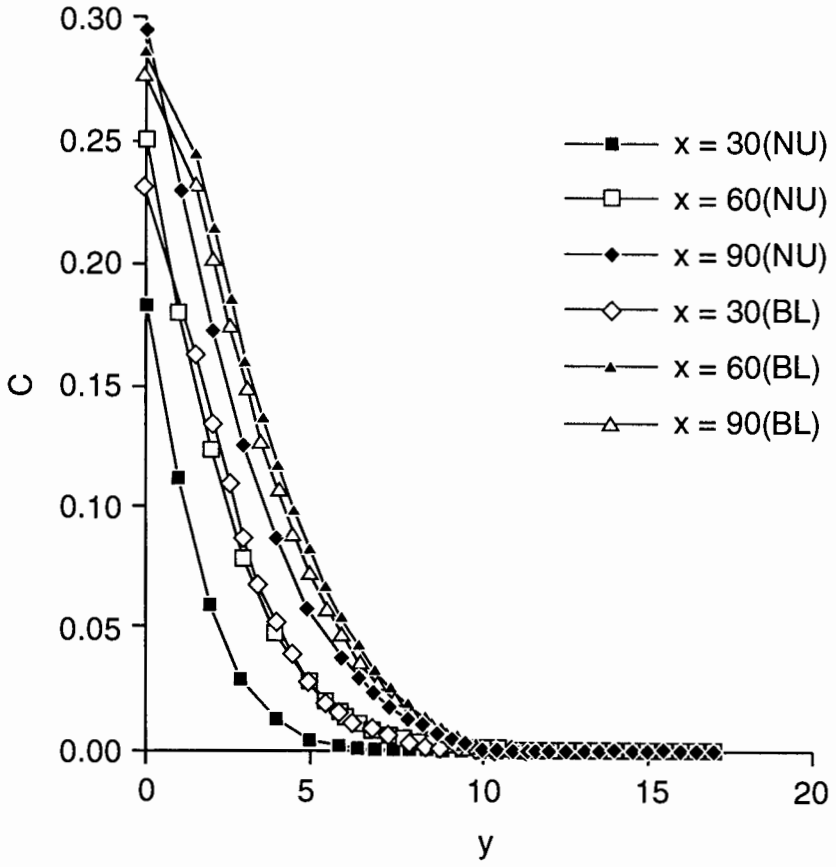

Fig. 7c Characteristics of the range $0 \leq x \leq x_{0.5}$ ($a = 0.1$, $q_R = 0.01$, $n = 3$)

(c) Salinity profiles

predictions with regard to values of δ and C_b. With regard to values of δ_0 and salinity profiles, the agreement was practically acceptable. It should be noted that values of δ_b could not be determined by the numerical method. The definition of δ_b is an artificial means of satisfying the boundary condition at $y = 0$. As long as δ_b is smaller than the vertical interval Δy of the numerical scheme, we can still consider that the numerical and BL approaches are compatible.

Figure 8 represents a single example of characterization of the range $x_{0.5} \leq x \leq x_e$. The results represented in Figs. 6 and 7 indicate that laws of similarity that are typical of BLs were least acceptable in this range of x-values. However, Fig. 8 shows quite good agreement between all predictions of the numerical and the BL methods for a rather long discontinuity in the impermeable layer, namely $x_e = 100$, while considering $n_1 = 1.3$ and $n_2 = 2.2$. These were simply some average values. The salinity profiles of Fig. 8(c) suggest that for large values of x_e the range $x_{0.5} \leq x \leq x_e$ might better be divided into some subranges in which values of n_1 and n_2 are subject to increase with x. However, even without such a division, Fig. 8 shows good agreement between the major parameters of the mineralization predicted by the numerical and the BL methods. It should be noted that changes of power coefficient laws require adjustment of BL parameters, to comply with mass conservation.

Characteristics of the range $x \geq x_e$ at a comparatively high value of q_R/a are depicted in Fig. 9. In this case matching between salinity profiles at $x_{0.5}$ and x_e is given by

$$
\begin{aligned}
(\delta_0)_{x_{0.5}^-} &= (\delta_0)_{x_{0.5}^+} \\
(\delta_b)_{x_{0.5}^-} &= (\delta_b)_{x_{0.5}^+} \\
(\delta_0)_{x_e^-} &= (\delta_0)_{x_e^+} \\
(\delta_u)_{x_e^-} &= (\delta_u)_{x_e^+}
\end{aligned}
\tag{77}
$$

where minus and plus superscripts of $x_{0.5}$ and x_e refer to upstream and downstream values, respectively. Some adjustments of the values given by eq. (77) are required to comply with mass conservation.

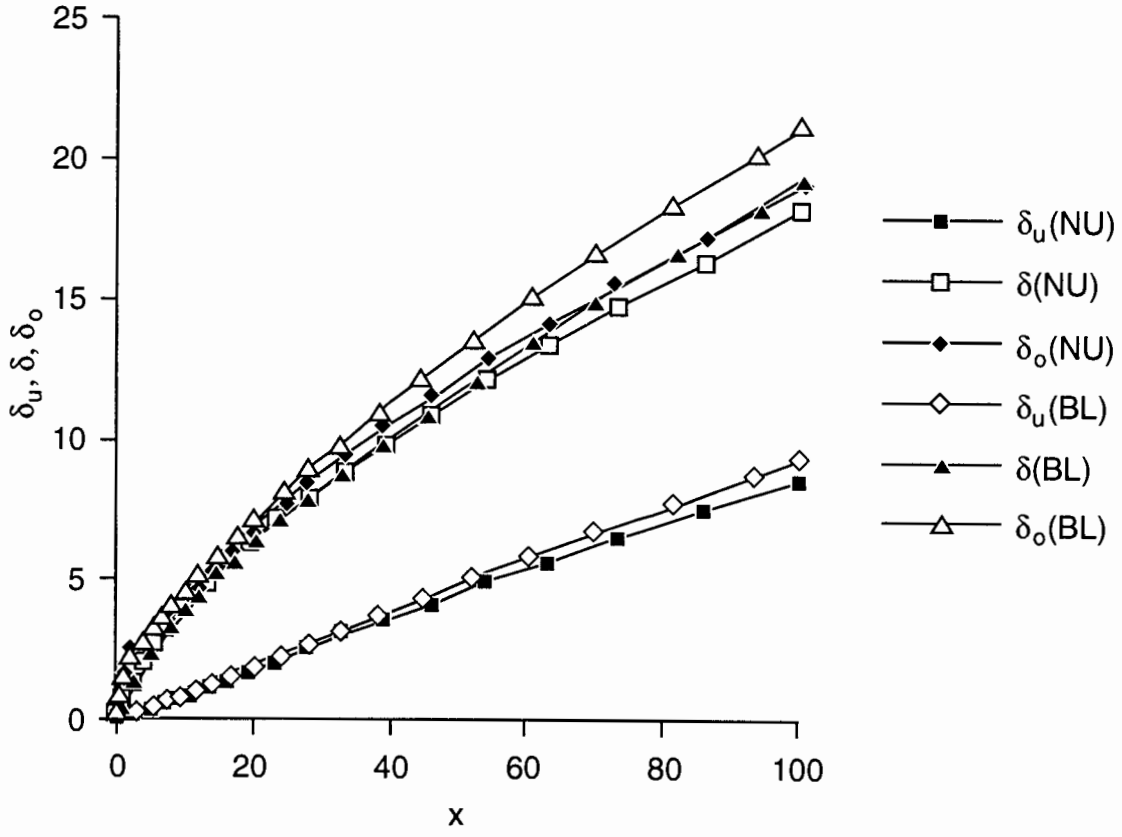

Fig. 8a Characteristics of the range $x_{0.5} \leq x \leq x_e$ ($a = 0.1$, $q_R = 0.1$, $n = 3$, $n_1 = 1.3$, $n_2 = 2.2$)

(a) Values of δ_b, δ, δ_0

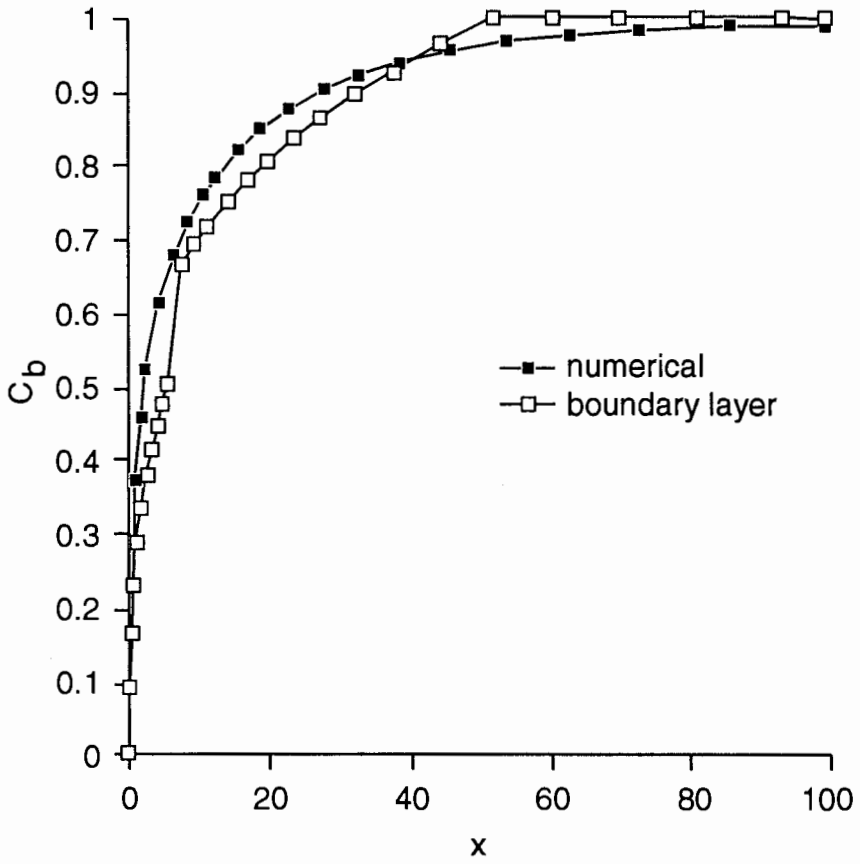

Fig. 8b Characteristics of the range $x_{0.5} \le x \le x_e$ ($a = 0.1$, $q_R = 0.1$, $n = 3$, $n_1 = 1.3$, $n_2 = 2.2$)

(b) Values of C_b

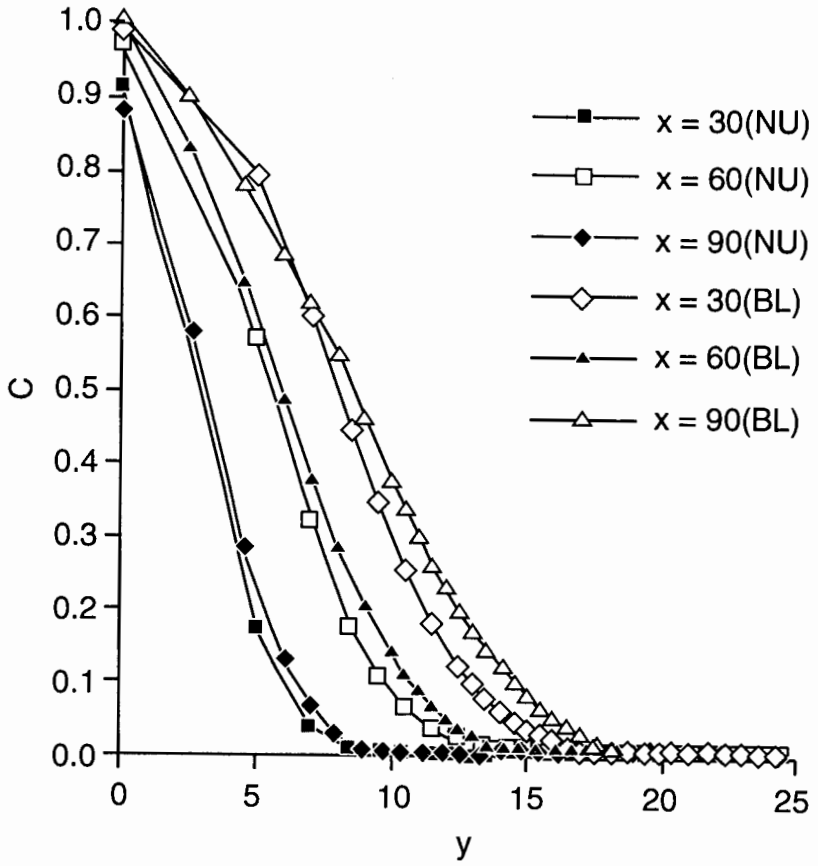

Fig. 8c Characteristics of the range $x_{0.5} \leq x \leq x_e$ ($a = 0.1$, $q_R = 0.1$, $n = 3$, $n_1 = 1.3$, $n_2 = 2.2$)

(c) Salinity profiles

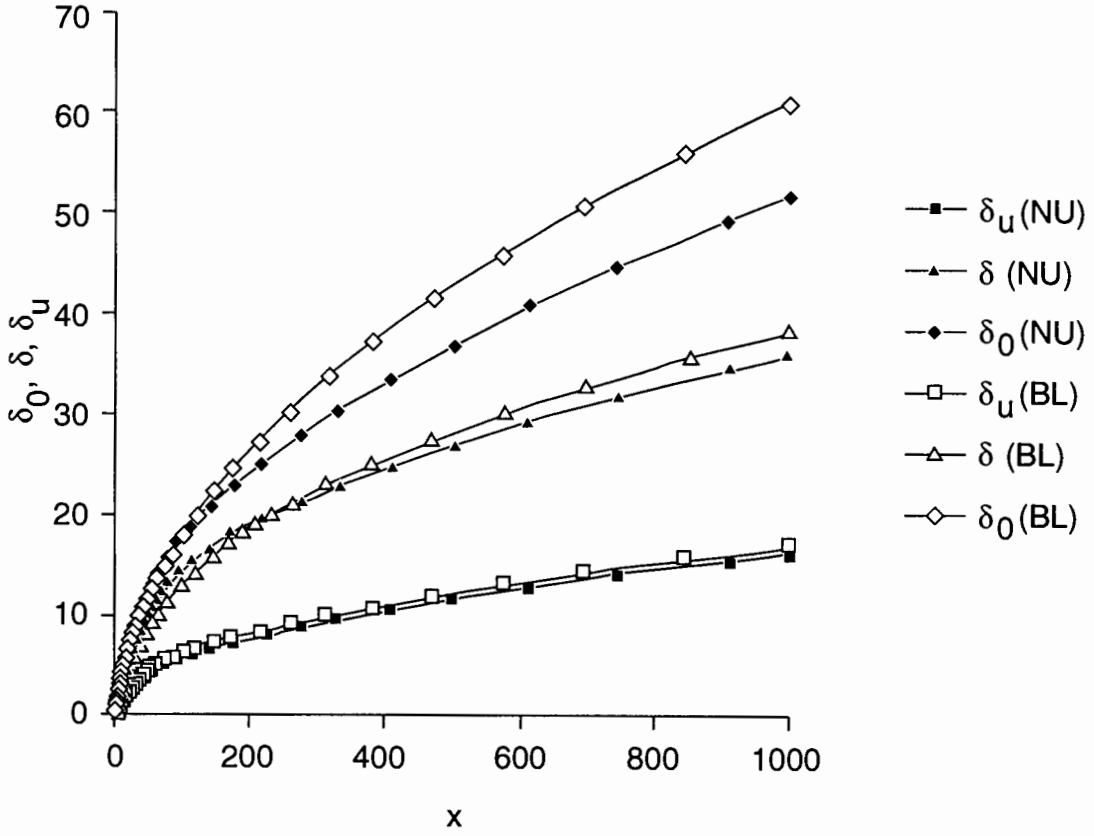

Fig. 9a Characteristics of the range $x \geq x_e$ at a high value of q_R/a ($a = 0.1$, $q_R = 0.1$, $x_e = 50$, $n = 3$, $n_1 = 1.3$, $n_2 = 2.2$, $n_3 = 1.84$, $n_4 = 4$)

(a) Values of δ_u, δ, δ_0

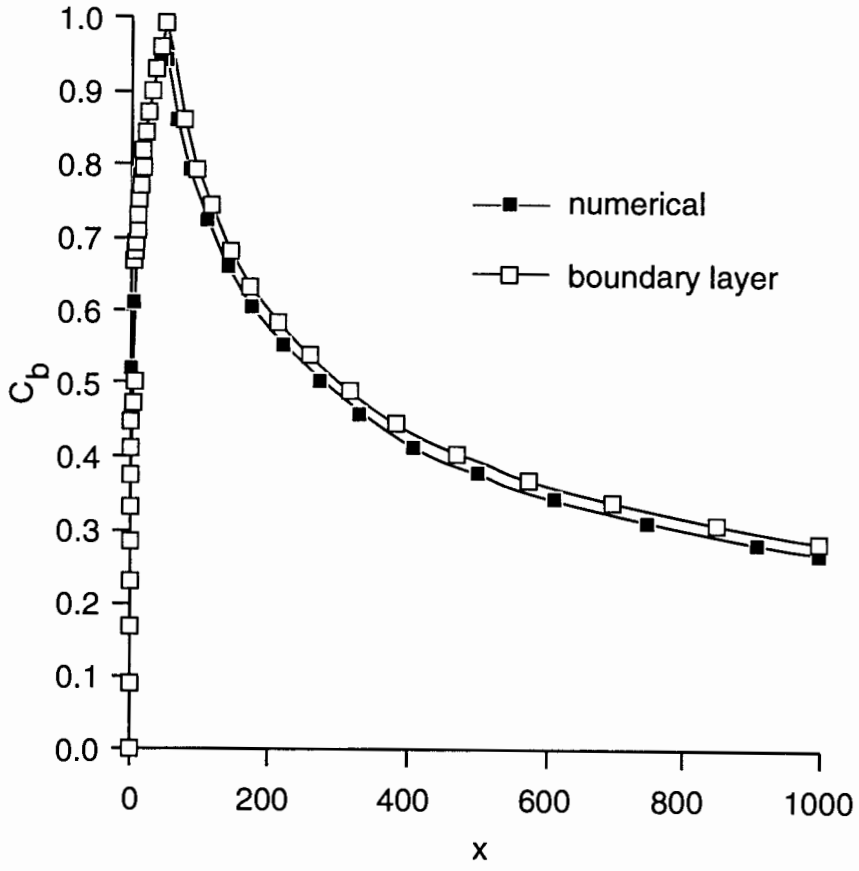

Fig. 9b Characteristics of the range $x \geq x_e$ at a high value of q_R/a ($a = 0.1$, $q_R = 0.1$, $x_e = 50$, $n = 3$, $n_1 = 1.3$, $n_2 = 2.2$, $n_3 = 1.84$, $n_4 = 4$)

(b) Values of C_b

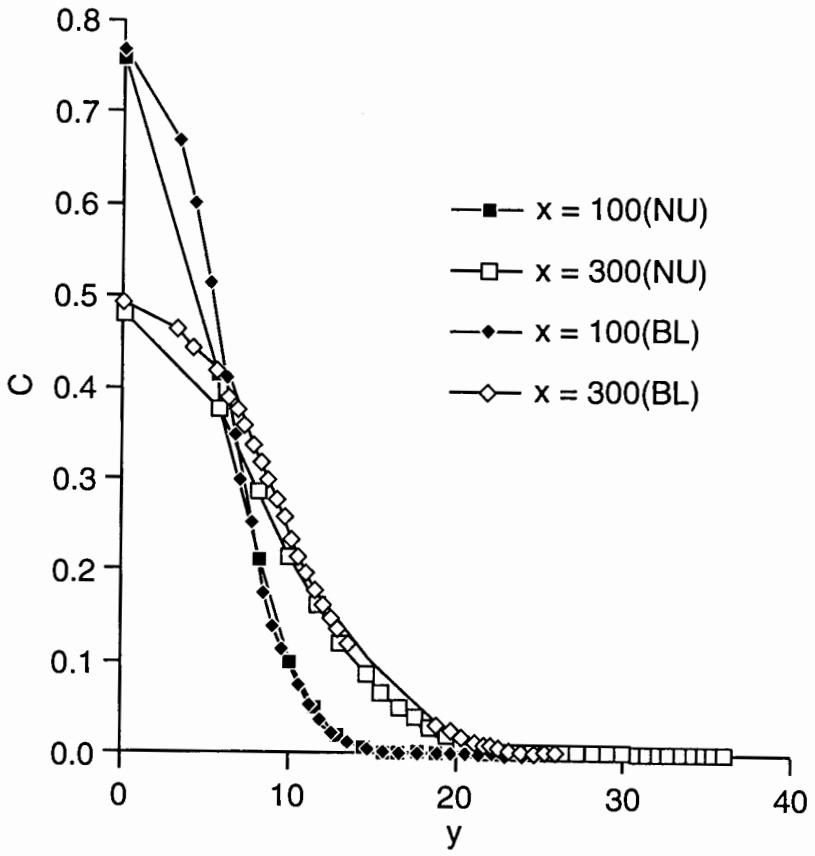

Fig. 9c Characteristics of the range $x \geq x_e$ at a high value of q_R/a ($a = 0.1$, $q_R = 0.1$, $x_e = 50$, $n = 3$, $n_1 = 1.3$, $n_2 = 2.2$, $n_3 = 1.84$, $n_4 = 4$)

(c) Salinity profiles

We also found it appropriate to apply:

$$n_3 = 1.84; \quad n_4 = 4 \tag{78}$$

as was obtained in report 1 and indicated by our preliminary numerical experiments.

The information assembled in Fig. 4 indicates that some difficulties could be expected in using the BL approach at comparatively high values of q_R/a like $q_R/a = 1$. However, Fig. 9 shows quite good agreement between the predictions of the numerical and the BL methods. This agreement is good with regard to all parameters of the mineralization process.

Figure 10 refers to characteristics of the mineralization process when the value of q_R/a is comparatively low, $q_R/a = 0.1$. According to Fig. 4, for such a small value of q_R/a the boundary layer approach is very appropriate. However, in the particular case of Fig. 10 the value of x_e was smaller than $x_{0.5}$. Therefore, appropriate measures had to be taken for adequate matching between the ranges $0 \le x \le x_{0.5}$ and $x \ge x_e$. We found that employment of the conservation of mass principle on both sides of x_e is a very appropriate matching procedure, namely

$$\left[\int_{y=0}^{y=\delta_u} C dy\right]_{x_e^-} = \left[\int_{y=0}^{y=\delta_u} C dy\right]_{x_e^+} \tag{79}$$

Introducing eq. (20) into the left-hand side and eq. (64) into the right hand side of eq. (79) and considering that at $0 \le y \le \delta_b$, the value of C was C_b, we obtained:

$$(\delta_u)_{x_e^+} = \left\{\delta_b\left(\frac{n_3+1}{n_3+C_r}\right)+(\delta_0-\delta_b)\frac{(n_3+1)\left[1-(1-\eta_u)^{n+1}\right]}{(n+1)(n_3+C_r)}\right\}_{x_e^-} \tag{80}$$

where

$$\eta_u = \left(\frac{\delta_u-\delta_b}{\delta_0-\delta_b}\right)_{x_e} \tag{81}$$

We applied eqs. (80) and (81) in simulations whose results are represented in Fig. 10, which shows very good agreement between the numerical and BL methods with regard to all parameters of the mineralization process.

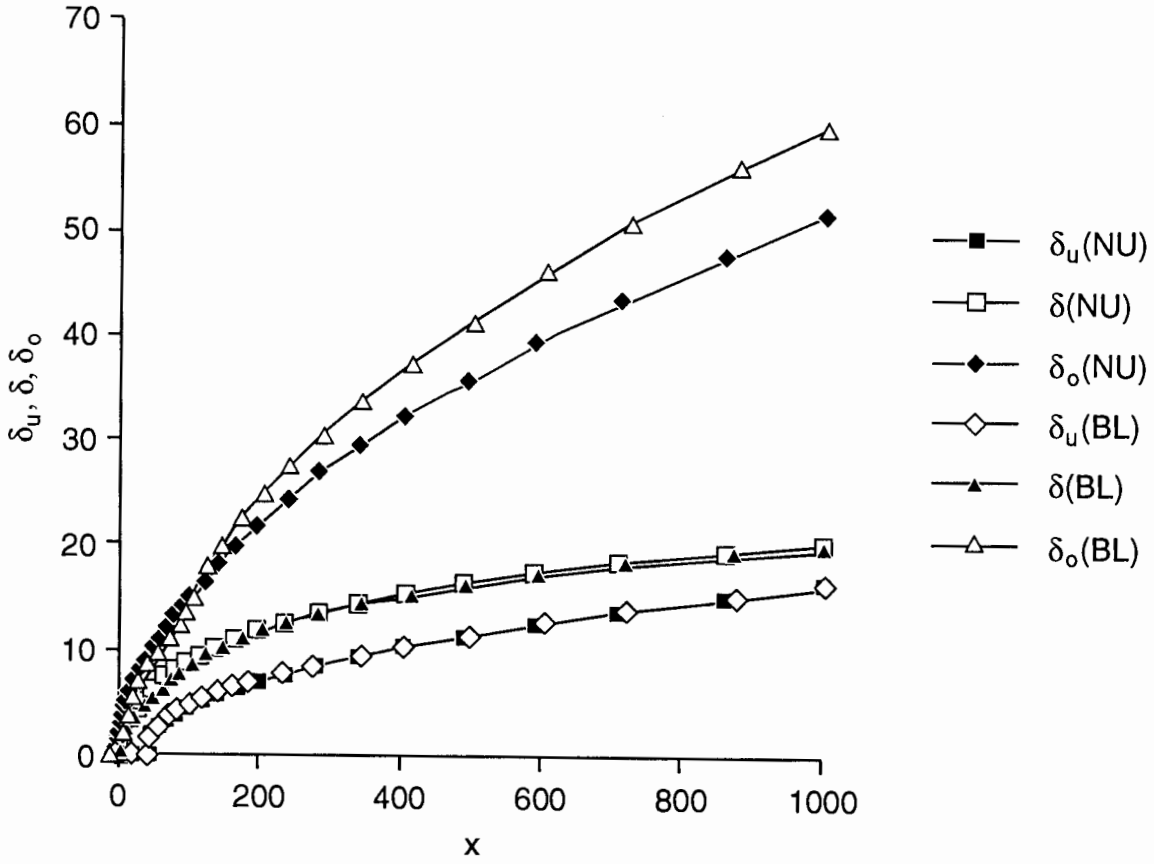

Fig. 10a Characteristics of the range $x \geq x_e$ at a low value of q_R/a ($a = 0.1$, $q_R = 0.01$, $x_e = 50$, $n = 3$, $n_1 = 1.3$, $n_2 = 2.2$, $n_3 = 1.84$, $n_4 = 4$)

(a) Values of δ_u, δ, δ_0

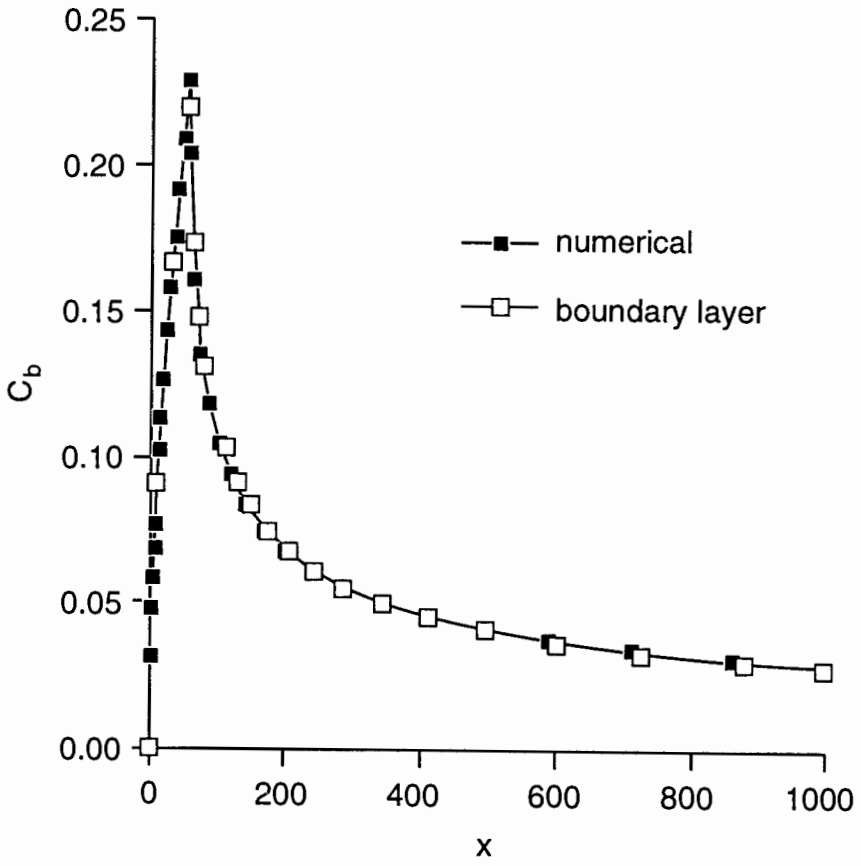

Fig. 10b Characteristics of the range $x \geq x_e$ at a low value of q_R/a ($a = 0.1$, $q_R = 0.01$, $x_e = 50$, $n = 3$, $n_1 = 1.3$, $n_2 = 2.2$, $n_3 = 1.84$, $n_4 = 4$)

(b) Values of C_b

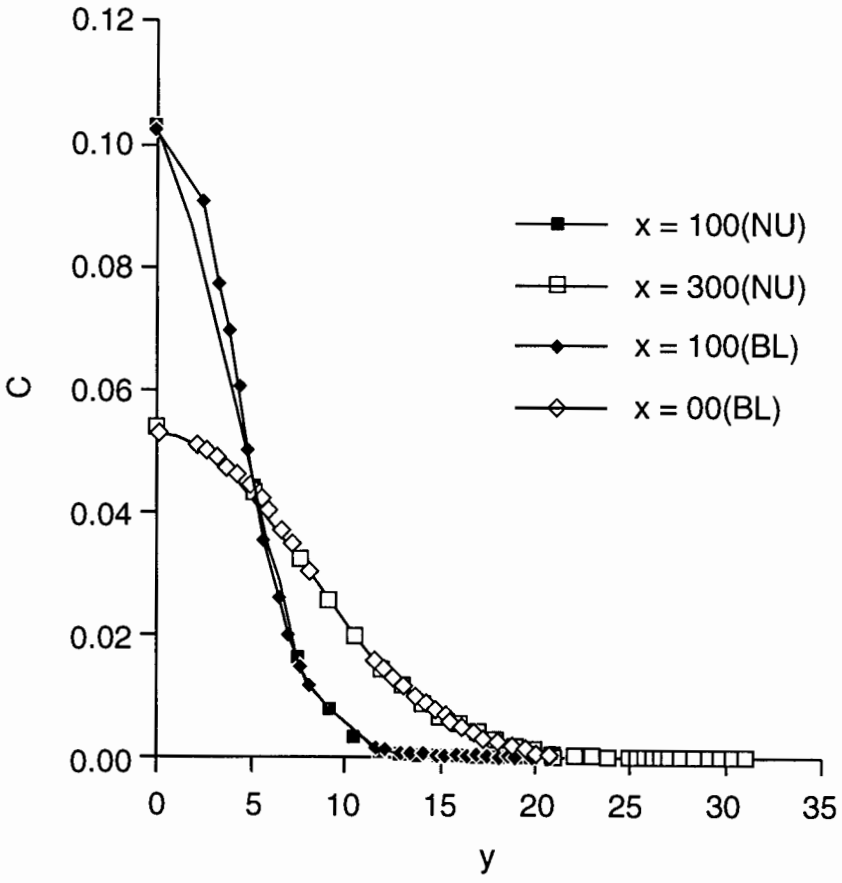

Fig. 10c Characteristics of the range $x \geq x_e$ at a low value of q_R/a ($a = 0.1$, $q_R = 0.01$, $x_e = 50$, $n = 3$, $n_1 = 1.3$, $n_2 = 2.2$, $n_3 = 1.84$, $n_4 = 4$)

(c) Salinity profiles

Fig. 11 shows the possible effect of the "saltwater mound" build-up. Fig. 5 indicated that at large values of q_R/a and x_e there might be some difficulties in the usage of the BL method developed in this paper. Such problems stem from the neglect of effects originating from the build-up of the "saltwater mound." Although in Fig. 5 we considered values of q_R/a up to q_R/a = 10, we assumed that practical values of this parameter in most of the relevant region of Kansas subject to groundwater mineralization are not larger than unity. We based this assumption on available geological information (Macfarlane et al., 1994) and considering that l_0 = 1m. Therefore, in Fig. 11 we referred to q_R/a = 1 and x_e = 100. Both of these values were assumed to be high values for practical applications. Generally, the results represented in Fig. 11 show good agreement between the numerical and BL predictions with regard to all parameters of the mineralization process. However, as indicated by Fig. 5, for higher values of q_R/a and x_e some more significant effects of the "saltwater mound" build-up were expected. Under such conditions usage of the BL approach developed in this paper could be considered as an extreme conservative prediction, as it magnifies the values of δ.

Figure 12 shows the steady state as well as the spearhead regions of the aquifer portion subject to mineralization and exemplifies the major parameter distributions along the entire extent of the salinity penetration, as predicted by the BL method developed in this report. We considered in this simulation that all BLs vanished at the front of the spearhead region where C_b was smaller than C_T. In initial stages, when C_b at x_e was smaller than 0.5, we applied eq. (80), in order to obtain an appropriate match between salinity profiles at x_e.

In should be noted that the BL method of the present study considers an aquifer of infinite thickness. When the predicted value of δ_0 is close to the thickness of the aquifer the salinity distribution starts to be affected by the top of the aquifer. Also, at a very large distance from the discontinuity of the impermeable layer, salinity distribution may become almost uniform in the vertical cross section. Such a result has not been obtained in the present study; it seems that such uniformity is usually obtained when the build-up of the BLs is affected by the top of the aquifer.

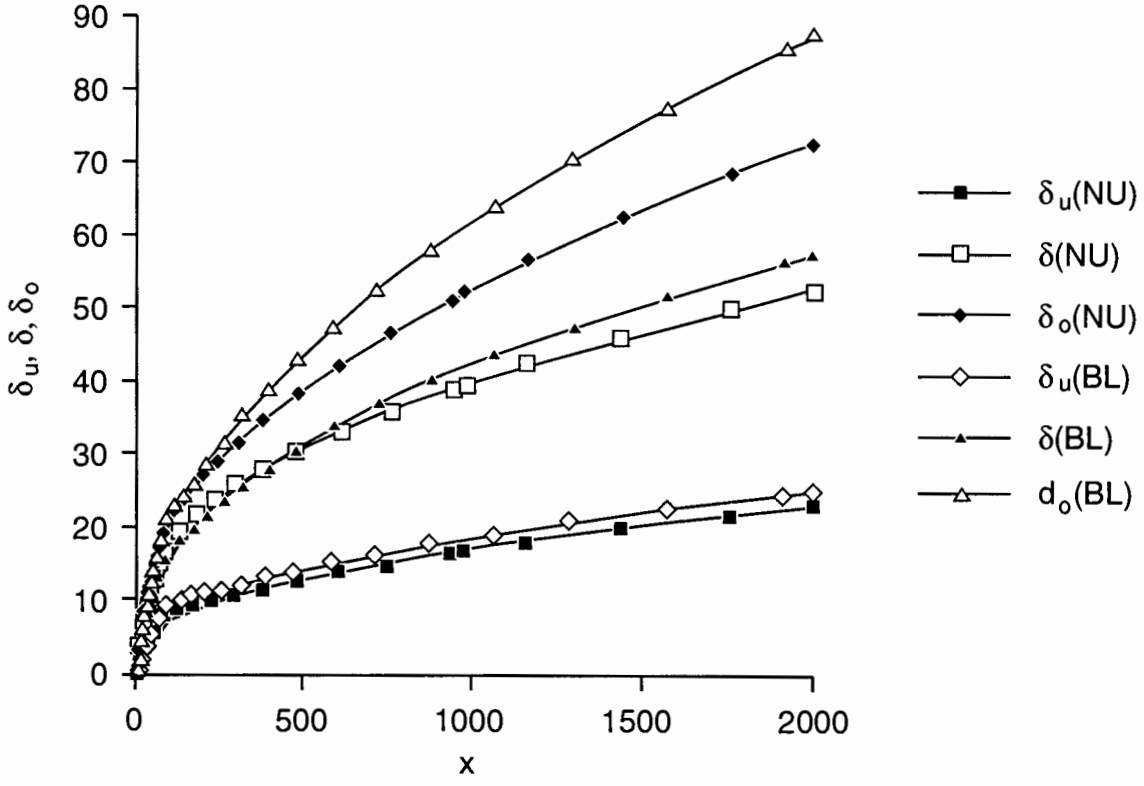

Fig. 11a Characteristics of the range $x \geq x_e$ at high values of q_R/a and x_e ($a = 0.1$, $q_R = 0.1$, $x_e = 100$, $n = 3$, $n_1 = 1.3$, $n_2 = 2.2$, $n_3 = 1.84$, $n_4 = 4$)

(a) Values of δ_u, δ, δ_0

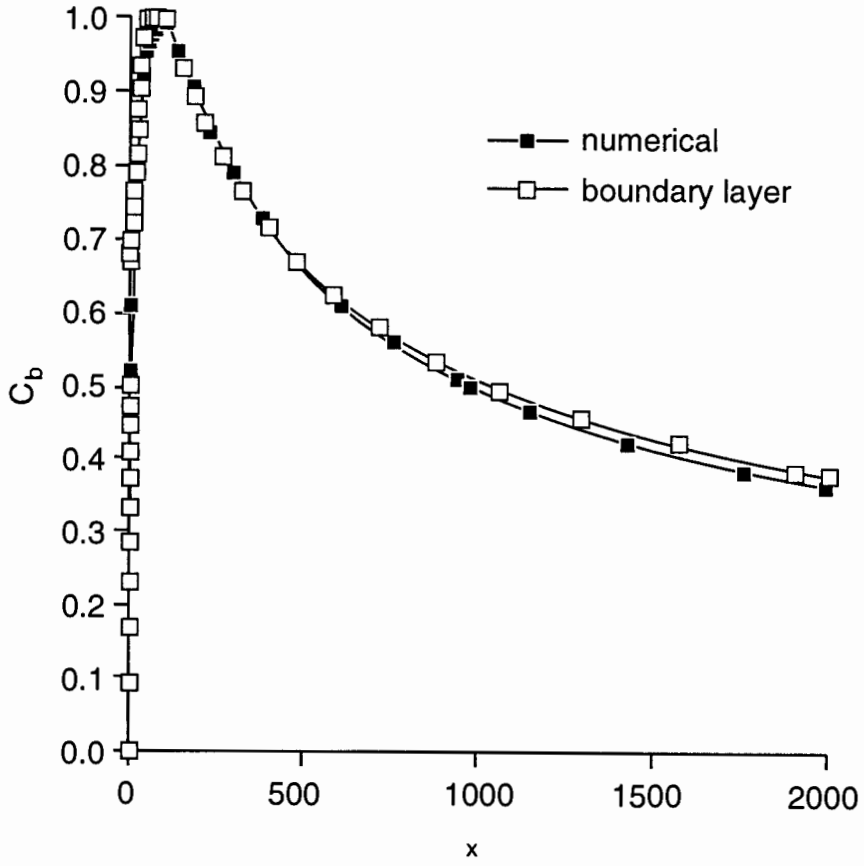

Fig. 11b Characteristics of the range $x \geq x_e$ at high values of q_R/a and x_e ($a = 0.1$, $q_R = 0.1$, $x_e = 100$, $n = 3$, $n_1 = 1.3$, $n_2 = 2.2$, $n_3 = 1.84$, $n_4 = 4$)

(b) Values of C_b

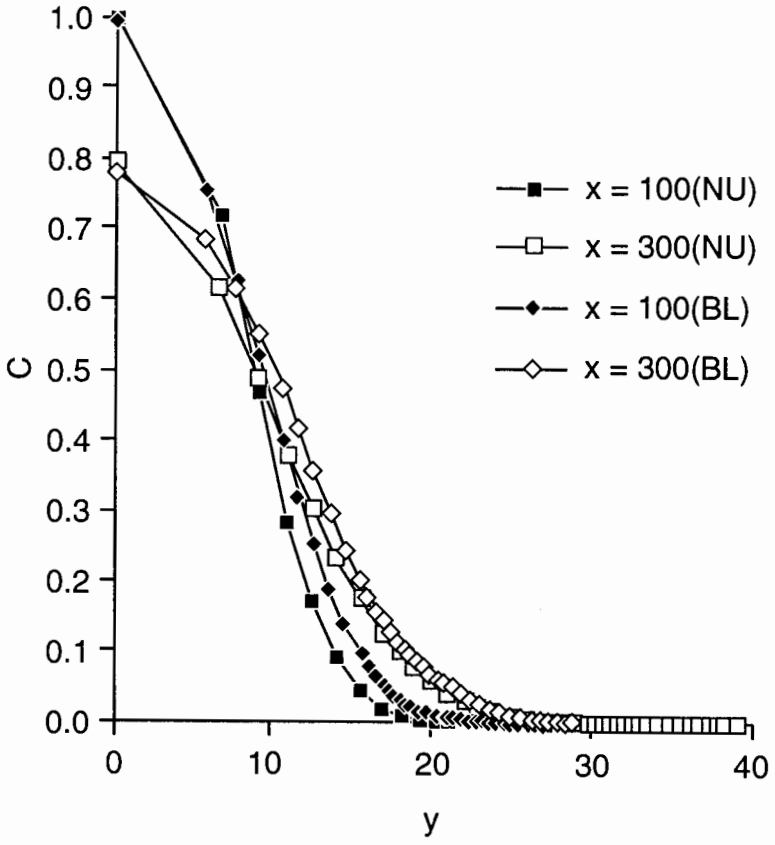

Fig. 11c Characteristics of the range $x \geq x_e$ at high values of q_R/a and x_e ($a = 0.1$, $q_R = 0.1$, $x_e = 100$, $n = 3$, $n_1 = 1.3$, $n_2 = 2.2$, $n_3 = 1.84$, $n_4 = 4$)

(c) Salinity profiles at $x = 100$, 300

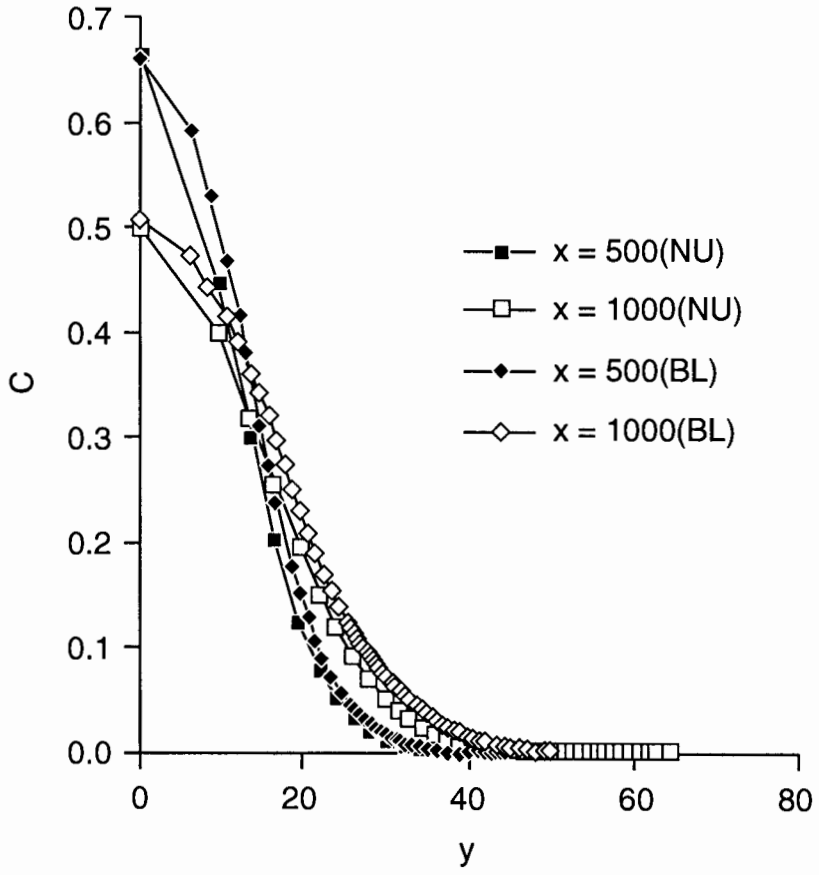

Fig. 11d Characteristics of the range $x \geq x_e$ at high values of q_R/a and x_e ($a = 0.1$, $q_R = 0.1$, $x_e = 100$, $n = 3$, $n_1 = 1.3$, $n_2 = 2.2$, $n_3 = 1.84$, $n_4 = 4$)

(d) Salinity profiles at $x = 500$, 1000

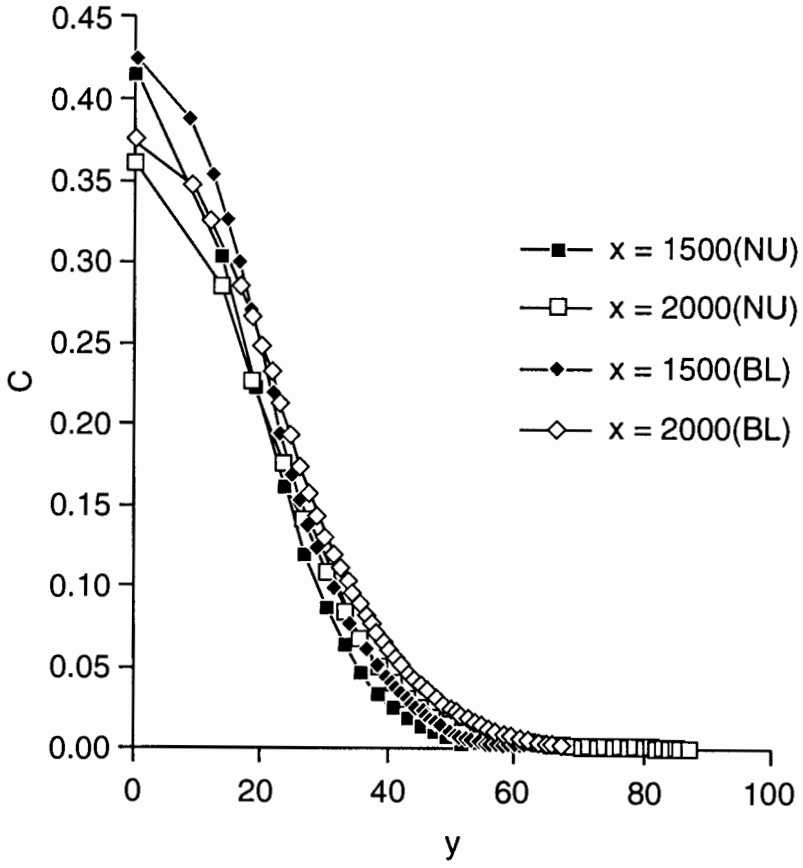

Fig. 11e Characteristics of the range $x \geq x_e$ at high values of q_R/a and x_e ($a = 0.1$, $q_R = 0.1$, $x_e = 100$, $n = 3$, $n_1 = 1.3$, $n_2 = 2.2$, $n_3 = 1.84$, $n_4 = 4$)

(e) Salinity profiles at $x = 1500$, 2000

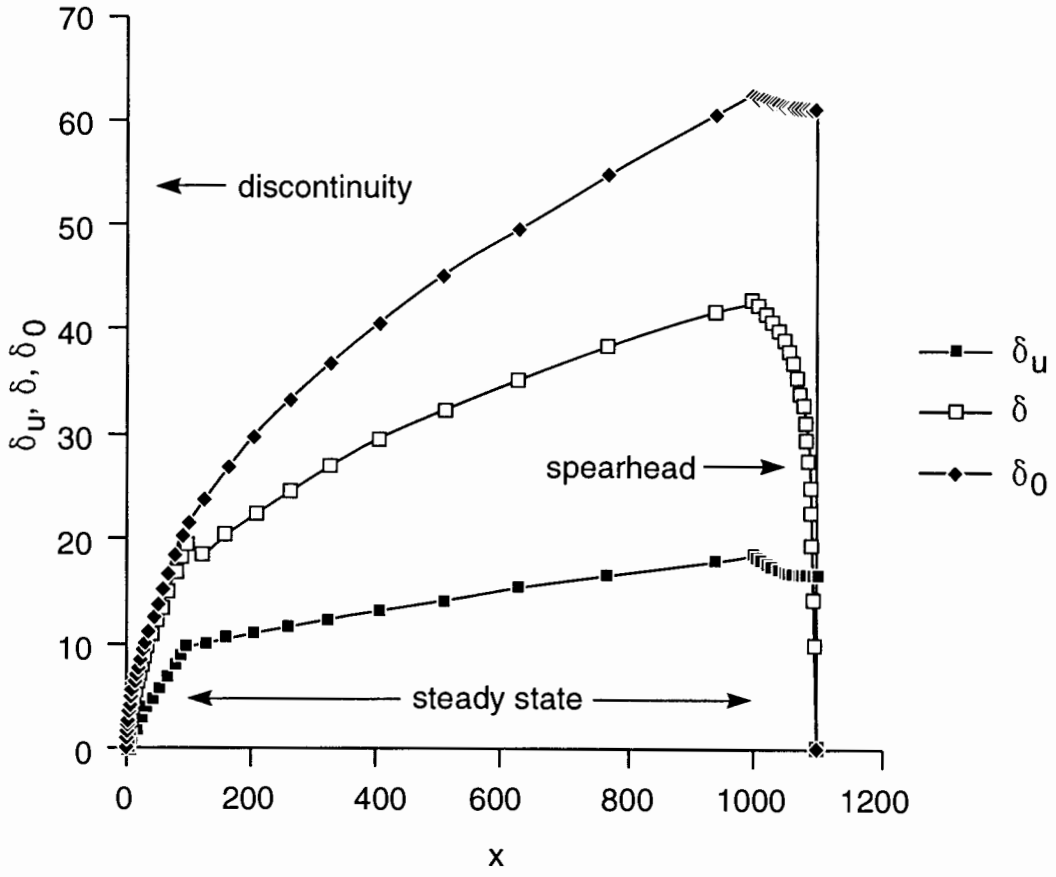

Fig. 12a Characteristics of the whole extent of the salinity penetration ($a = 0.1$, $q_R = 0.1$, $x_e = 100$, $t = 1100$, $n = 3$, $n_1 = 1.3$, $n_2 = 2.2$, $n_3 = 1.84$, $n_4 = 4$)

(a) Shape of the various boundary layers

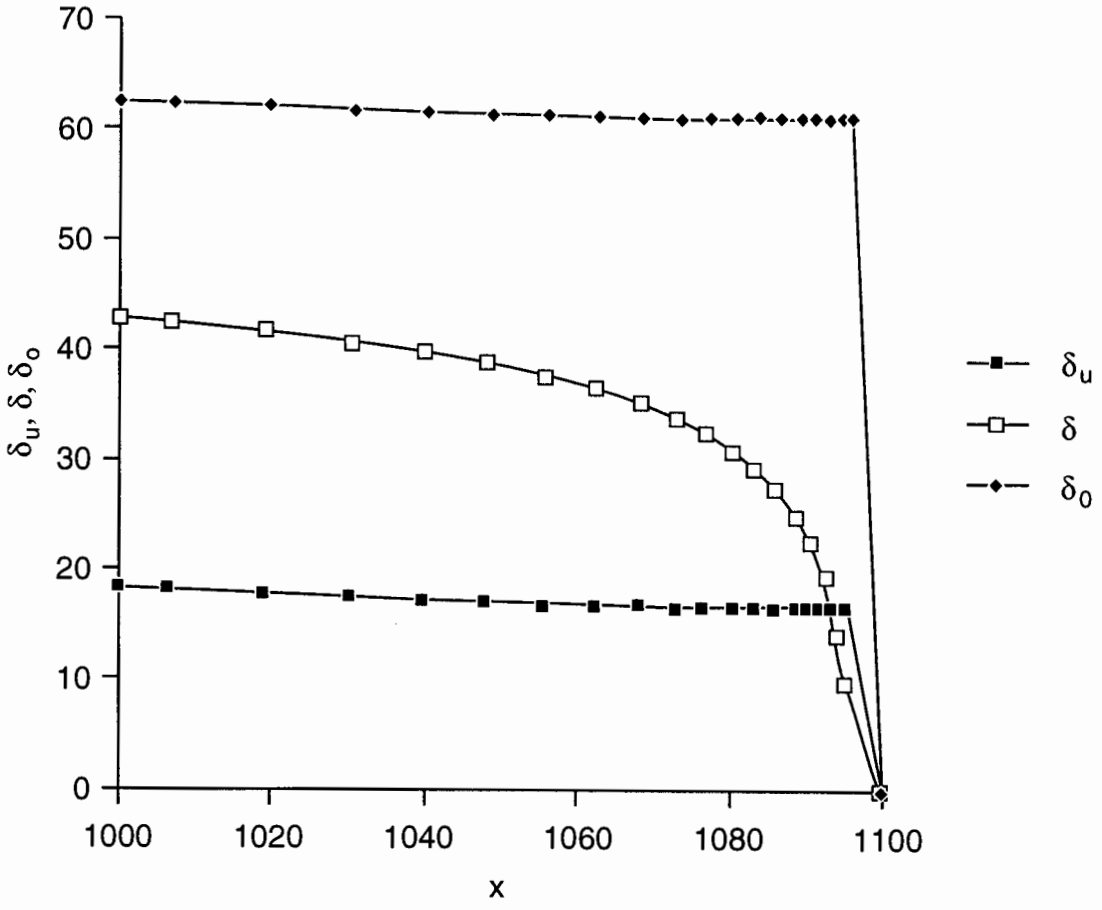

Fig. 12b Characteristics of the whole extent of the salinity penetration ($a = 0.1$, $q_R = 0.1$, $x_e = 100$, $t = 1100$, $n = 3$, $n_1 = 1.3$, $n_2 = 2.2$, $n_3 = 1.84$, $n_4 = 4$)

(b) Boundary layers at the spearhead region

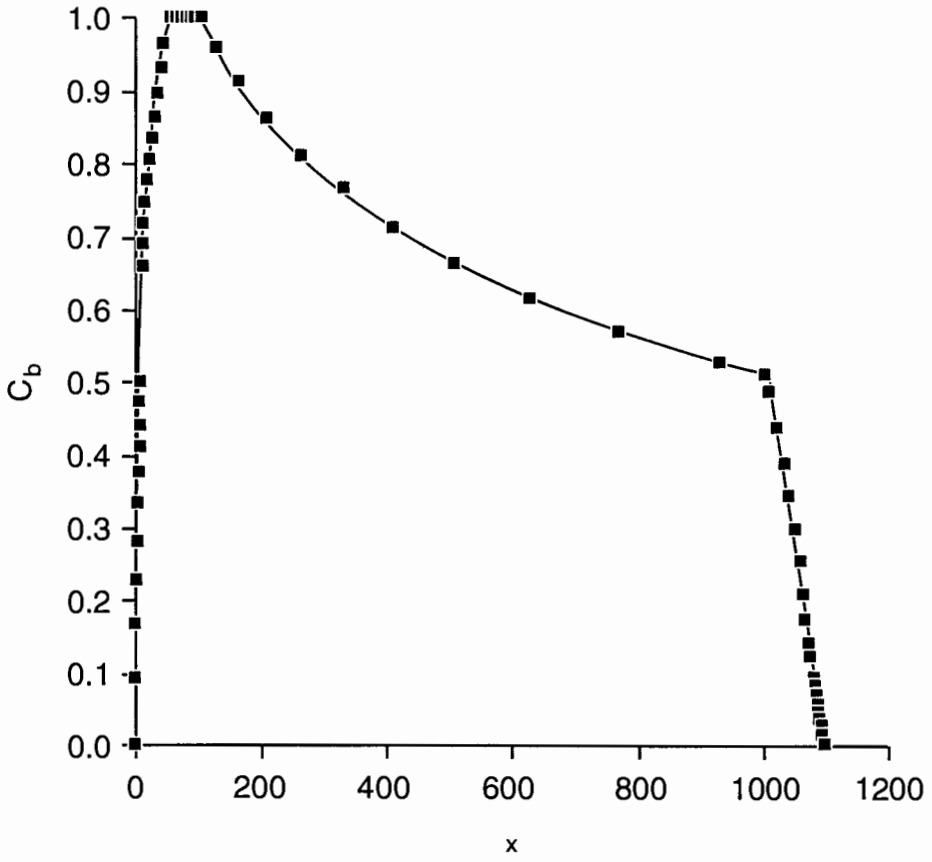

Fig. 12c Characteristics of the whole extent of the salinity penetration ($a = 0.1$, $q_R = 0.1$, $x_e = 100$, $t = 1100$, $n = 3$, $n_1 = 1.3$, $n_2 = 2.2$, $n_3 = 1.84$, $n_4 = 4$)

(c) Distribution of C_b

Some practical applications

The method developed in this study has already been applied to the estimate of some phenomena associated with aquifer mineralization in Kansas. Garneau (1995) analyzed measurements of salinity in sets of monitoring wells, some of them drilled in regions subject to seepage of saline water from the deep formation into the freshwater aquifer. Other monitoring wells were located downstream of the area of saline water seepage. Therefore he could follow the development of salinity profiles in various east-west cross sections of the aquifer. In his study he applied the methods developed in the previous studies (Rubin and Buddemeier, 1998a, b) and the method of the present study. As mentioned in report 1, he could analyze salinity profiles in locations of direct contact between the saline and freshwater as well as profiles measured downstream of such locations. By comparing the field measurements with the TSBL method he found values of the characteristic transverse dispersivities of the aquifer. He could also estimate the location of discontinuities of the impermeable layer.

Young and Rubin (1998) have calculated possible infiltration of saline water from the deep bedrock into the freshwater aquifer, in locations of salinity penetration into the freshwater aquifer. They made measurements of salinity profiles in closely-spaced monitoring wells that penetrated to various depths in the aquifer as well as into the bedrock surface. They measured the pressure in all wells at particular locations, and made an integration of the density profile, to calculate the "effective hydrostatic pressure" in the bedrock aquifer. According to the difference between the measured pressure in the bedrock aquifer and its effective hydrostatic pressure, as well as the approximate value of the vertical hydraulic conductivity, Young and Rubin (1998) calculated the rate of seepage of salt water from the bedrock aquifer to the freshwater zone. Calculations of Young and Rubin (1998) and Garneau (1995) can be used to obtain better estimates of dispersivity values, as well as the size of the discontinuity, through which saline water seeps into the freshwater aquifer.

Quinodoz and Buddemeier (1997) calculated budgets of groundwater and salinity in sections of the aquifer subject to mineralization. Their calculations could verify, and be used for

checking the validity of, some of the estimated calculations of Young and Rubin (1998) and Garneau (1995).

Summary and Conclusions

Recent studies have shown that in many cases of aquifer mineralization in South-central Kansas, saltwater seeps into the freshwater aquifer through semiconfining discontinuities in impermeable layers.

In the framework of this study a method employing the top specified boundary layer (TSBL) was developed for the prediction of the salinity penetration into the freshwater aquifer through such semiconfining discontinuities in an impermeable layer. The method considered two ranges of x-values at the discontinuity in the impermeable layer and two ranges of x-values downstream of that discontinuity.

Ranges within the discontinuity were:

(a) x-values for which C_b was smaller than 0.5, and

(b) x-values for which C_b was larger than 0.5.

Ranges of x-values downstream of the discontinuity were:

(a) the steady state region extending between $x = x_e$ and $x = t$, and

(b) the spear-head region extended between $x = t$ and $x = t + x_e$.

In range (a) within the discontinuity it was assumed that a bottom BL and an outer BL developed. Salinity distribution in the bottom BL was uniform. In the outer BL, salinity distribution was represented by a power series expansion.

In range (b) of the discontinuity it was assumed that inner and outer BLs developed. In both layers salinity distributions were represented by power series expansions.

The range of x-values downstream of the discontinuity was simulated by a single model, which assumed that inner and outer BLs developed in that domain. In both layers salinity distributions were represented by series expansions. There was no salinity transfer between the

BLs, and the vertical salinity gradients led to the expansion of the two BLs. Good agreement was obtained between results of the BL method of this study and numerical simulations for predictions of major mineralization parameters.

The BL method defined major parameters of the mineralization process. The most important parameter was the top specified boundary layer (TSBL) which identifies the region of interest (ROI). In the ROI the salinity was larger than the acceptable value. Other major parameters were the value of the salinity at the bottom of the aquifer and the salinity distribution in the ROI.

The method developed in this study was found to be applicable up to $q_R/a = 1$ and $x_e = 100$. At higher values of these parameters, effects of the build-up of a "saltwater mound" at the discontinuity were observed. Use of the BL method when such effects are significant can be assumed to be a conservative approach, as the BL calculation magnifies the vertical expansion of the salinity penetration under such conditions.

The BL method developed in this study represents a quick approach for the characterization of the mineralization process by the employment of a set of small number of simply defined major parameters.

ACKNOWLEDGMENTS

This work was supported under contracts between the Kansas Water Office and the Kansas Geological Survey. The authors are grateful for the assistance of Mark Schoneweis in preparing the illustrations.

Notation

a	dimensionless transverse dispersivity
a_L	dimensionless longitudinal dispersivity
BL	boundary layer c_r ratio between C and C_b at the boundary between the inner and outer boundary layers
C	dimensionless salinity
C_b	dimensionless salinity at the bottom of the aquifer
C_T	dimensionless salinity at the top of the ROI
C^*	salt concentration (– salinity) [ML^{-3}]
C_f^*	salinity of the freshwater [ML^{-3}]
C_s^*	salinity of the saltwater [ML^{-3}]
$\tilde{D}$	dispersion tensor [L^2T^{-1}]
D_x	longitudinal dispersion coefficient [L^2T^{-1}]
D_y	transverse dispersion coefficient [L^2T^{-1}]
f	a function defined in eq. (61)
F	a function defined in eq. (60)
G	a function defined in eq. (30)
H	a function defined in eq. (32)
g	gravitational acceleration [LT^{-2}]
i	number of nodal point in the longitudinal direction
j	number of nodal point in the vertical direction
k	permeability [L^2]
l_0	length scale [L]
L	power series functions defined in eqs. (50) and (67)
M	power series functions defined in eqs. (46) and (65)
n	power coefficient of boundary layer series expansion at $0 \le x \le x_{as}$
(n)	number of iteration

n_1	power coefficient of inner boundary layer at $x_{o,s} \leq x \leq x_s$
n_2	power coefficient of outer boundary layer at $x_{o,s} \leq x \leq x_s$
n_3	power coefficient of inner boundary layer at $x > x_e$
n_4	power coefficient of outer boundary layer at $x > x_e$
NU	value obtained by numerical simulation
p	pressure [MLT^{-2}]
q	specific discharge [LT^{-1}]
q_0	specific discharge of the aquifer at $x = 0$ [LT^{-1}]
q_S	specific discharge of the seeping saltwater [LT^{-1}]
q_R	ratio between q_S and q_0
ROI	region of interest
t	dimensionless time
t_e	the dimensionless time needed by a fluid particle to be advected from x_e to x
t^*	time (T)
TSBL	top specified boundary layer
u	dimensionless longitudinal velocity
U	longitudinal interstitial flow velocity [LT^{-1}]
U_0	value of U at $x \leq 0$ [LT^{-1}]
v	dimensionless vertical velocity
V	vertical interstitial flow velocity [LT^{-1}]
x	dimensionless longitudinal coordinate
x^*	longitudinal coordinate [L]
x_b	starting point for the ROI build-up
$x_{0.5}$	starting point for $C_b \geq 0.5$
x_e	dimensionless length of the impermeable layer discontinuity
x_{max}	maximum value of x incorporated in the simulation
x_e^*	length of the discontinuity [L]

y	dimensionless vertical coordinate
y_{max}	maximum value of y incorporated in the numerical simulation
y^*	vertical coordinate [L]
α_1	coefficient defined in eq. (68)
α_2	coefficient defined in eq. (69)
$a_i (i = 0,\ldots,4)$	coefficients defined in eq. (15)
$\beta_i (i = 0,\ldots,2)$	coefficients defined in eq. (10)
$\gamma_i (i = 0,\ldots,4)$	coefficients defined in eq. (12)
δ	dimensionless thickness of the ROI
δ_b	dimensionless thickness of the bottom boundary layer
δ_u	dimensionless thickness of the inner boundary layer
δ_0	dimensionless thickness of the combined outer and inner boundary layer
δ_R	ratio between δ_0 and δ_u
Δx	longitudinal interval
Δy	vertical interval
η	outer boundary layer coordinate
η_T	value of η at $y = \delta$
η_u	value of η defined in eq. (81)
μ	viscosity [$ML^{-1}T^{-1}$]
ξ	inner boundary layer coordinate
ξ_T	value of ξ at $y = \delta$
ϕ	porosity
Φ	dimensionless potential function
ρ	fluid density [ML^{-3}]
ρ_f	density of the freshwater [ML^{-3}]
τ	modified coordinate equal to $\delta_0 - \delta_b$
τ_b	value of τ at x_b

ω	over-relaxation coefficient

References

Buddemeier, R.W., Garneau, G.W., Young, D.P., Whittemore, D.O., Zehr, D., Lanterman, J., Ma, T.S., and Falk, S., 1994. The mineral intrusion project: Progress and activities during fiscal year 1994, Open-File Rept. 94-28, Geohydrology, Kansas Geological Survey, The University of Kansas, Lawrence, KS.

Carslaw, H.S. and Jaeger, J.C., 1959. Conduction of Heat in Solids. Oxford at the Clarendon Press, London.

Fischer, H.B., List, E., Koh, R.C.Y., Imberger, J. and Brooks, N.H., 1979. Mixing in Inland and Coastal Waters, Academic Press, NY.

Garneau, G.W., 1995. Detection and characterization of the distribution of mineral intrusion in the Great Bend Prairie Aquifer – south-central Kansas, Kansas Geological Survey Open-File Report 95-35,The University of Kansas, Lawrence, KS.

Lapidus, L., and Pinder, G.F., 1982. "Numerical Solution of Partial Differential Equations in Science and Engineering," John-Wiley & Sons, NY.

Macfarlane, P.A., Combes, J., Turbek, S., and Kirshen, D., 1993. Shallow subsurface bedrock geology and hydrostratigraphy of southwestern Kansas, Open-File Rept. 93-1A, Kansas Geological Survey, The University of Kansas, Lawrence, KS.

Rubin, H., and Buddemeier, R.W., 1996. A top specified boundary layer (TSBL) approximation approach for the simulation of groundwater contamination processes, Journal of Contaminant Hydrology, 22: 123 – 144.

Rubin, H., and Buddemeier, R.W., 1998a. Application of the top specified boundary layer (TSBL) approximation to initial characterization of an inland aquifer mineralization, Part 1: Direct contact between fresh and saltwater, Journal of Contaminant Hydrology , 32/3-4: 149-172.

Rubin, H., and Buddemeier, R.W., 1998b. Application of the top specified boundary layer (TSBL) approximation to initial characterization of an inland aquifer mineralization, Part 2: Seepage of saltwater, Journal of Contaminant Hydrology, 32/3-4, 173-198.

Rubin, H., and Buddemeier, R.W., 1998c. Approximate analysis of groundwater mineralization due to local discontinuity in impermeable layer - Part. 1: Direct contact between fresh and saltwater. Kansas Geological Survey Open-File Report 98-31, The University of Kansas, Lawrence, KS.

Young, D. and Rubin, H., 1998. Determining vertical flow in variable density groundwater - a hydrostatic approach applied in south-central Kansas, Eighteenth Annual Hydrology Days, Colorado State University, Fort Collins, Colorado, March 30-April 3, 1998.